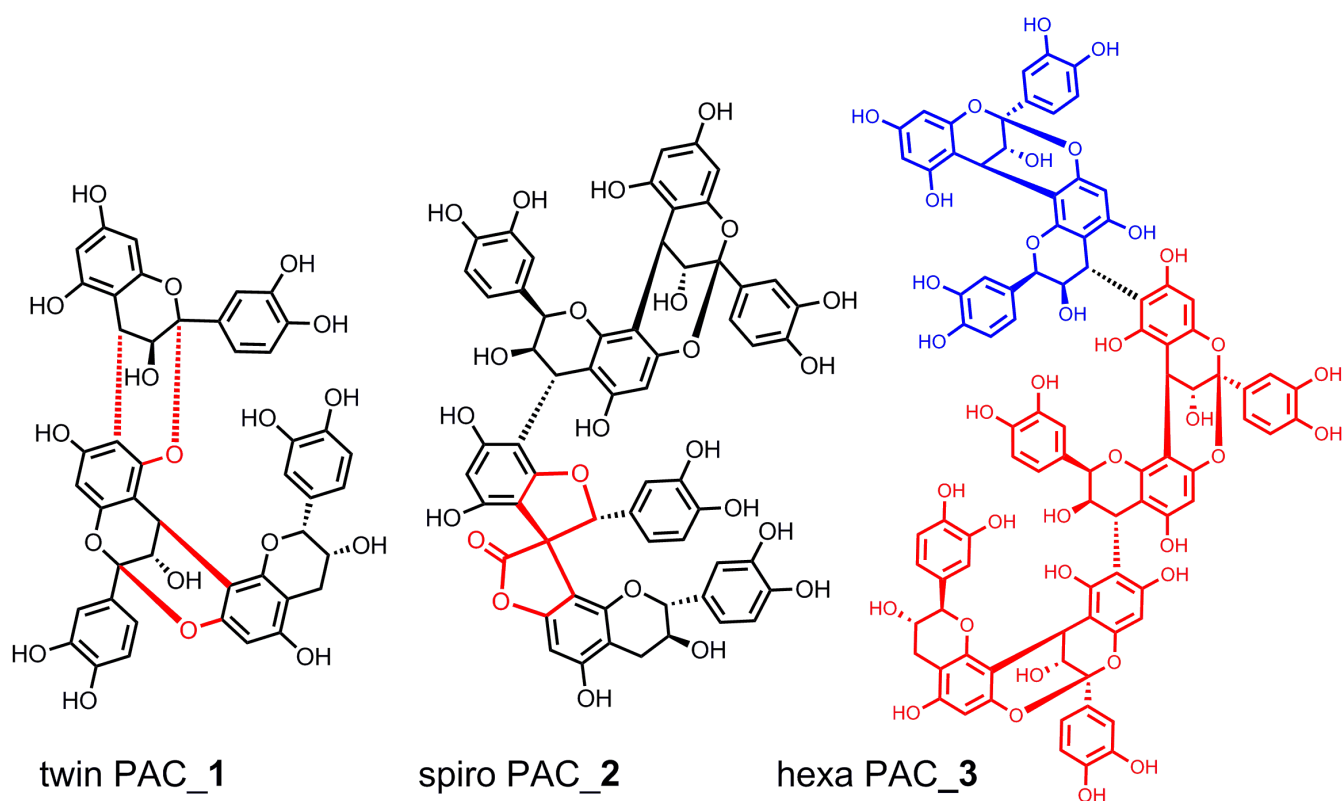


Rare A-Type, New Spiro-Type, and Highly Oligomeric Proanthocyanidins from *Pinus massoniana*

Bin Zhou^{1,†}, Yvette Alania^{3,4}, Mariana C. Reis^{3,4}, James B. McAlpine^{1,2}, Ana K. Bedran-Russo^{2,3,4}, Guido F. Pauli^{1,2}, and Shao-Nong Chen^{1,2,*}

¹Department of Pharmaceutical Sciences and ²Program for Collaborative Research in the Pharmaceutical Sciences (PCRPS), College of Pharmacy, ³Department of Restorative Dentistry, College of Dentistry, University of Illinois at Chicago, Chicago, Illinois 60612, USA; ⁴Department of General Dental Sciences, School of Dentistry, Marquette University, Milwaukee, Wisconsin 53233, USA



ABSTRACT: Isolation of underivatized PACs led to three new, structurally unique PACs (**1–3**) from pine bark. Pinutwindoubilin (**1**) is the first known trimer with double A-type interflavanyl linkages ($2\alpha\rightarrow O\rightarrow 5,4\alpha\rightarrow 6$ and $2\alpha\rightarrow O\rightarrow 7,4\alpha\rightarrow 8$). Pinuspirotetrin (**2**) represents the first PAC tetramer with a heterodimeric framework consisting of one spiro-type and one A-type dimer. Pinumassohexin (**3**) was elucidated as a mixed A + B type hexamer that consists of the tetramer, peanut procyanidin E, and an A-type dimer (**5**).

The bark of the pine species, *Pinus massoniana*, is a rich source of proanthocyanidins (PACs), a phylogenetically ancient group of polyphenols that occur ubiquitously in vascular plants. Accordingly, PACs inevitably impact human life via nutrition and medicine. Representing a group of vast structural diversity, PACs exhibit a broad spectrum of bioactivities.^{1–7} Specific to pine bark, a series of tri- and tetrameric PACs has the demonstrated capability of enhancing the biomechanical properties of dentin and

[†]**Present Address:** State Key Laboratory of Drug Research, Shanghai Institute of Materia Medica, Chinese Academy of Sciences, 555 Zuchongzhi Road, Shanghai 201203, People's Republic of China

instill resistance to proteolytic dentin degradation.^{6,7} Continuing these interdisciplinary efforts at the interface of natural products chemistry and dentistry, exploration of structurally unique compounds from bioactive PAC oligomer fractions led to three structurally distinctive new PACs (**1–3**) (Figure 1).

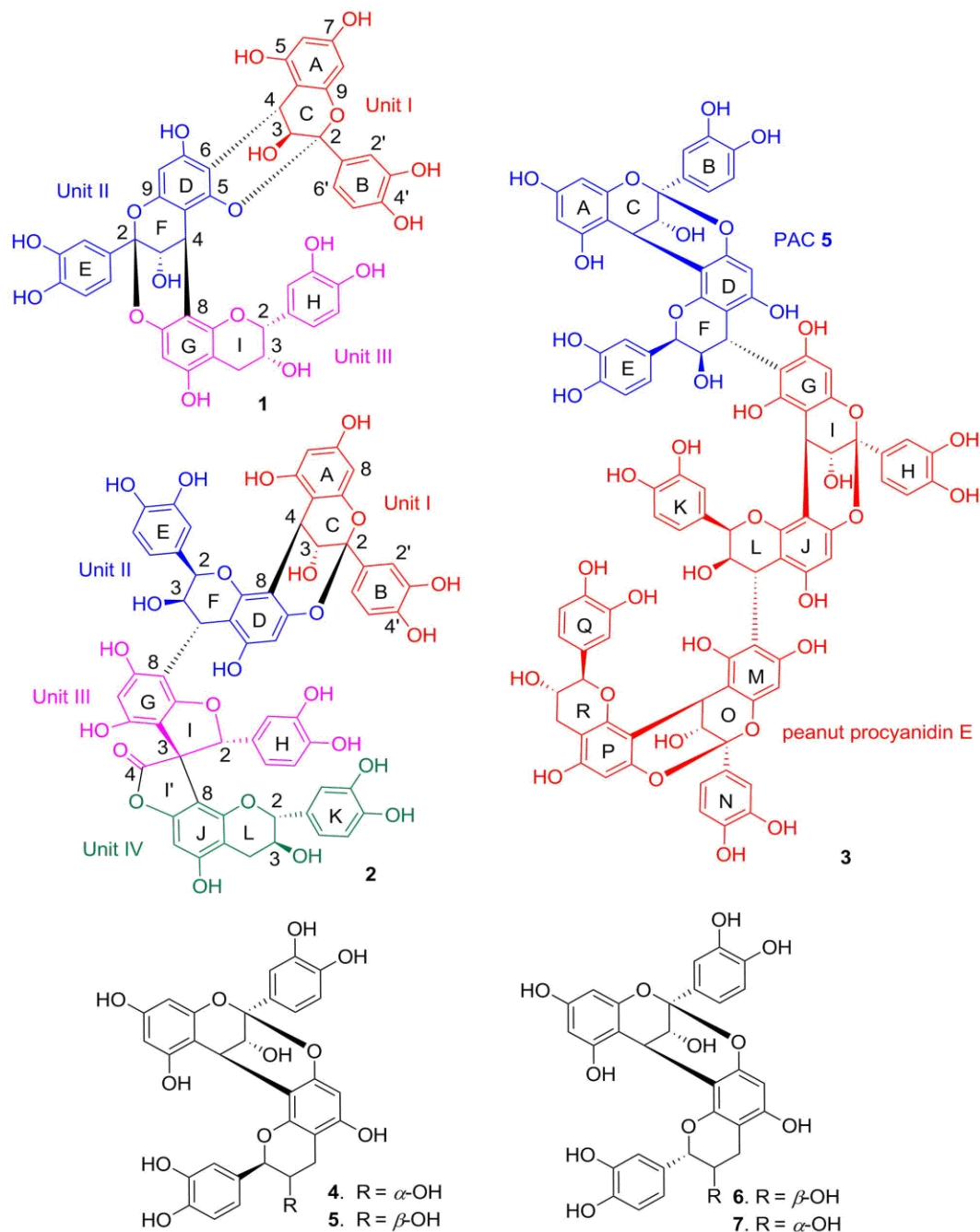


Figure 1. Novel structures **1–3** with color coded constituent catechol monomers, compared with the known dimers, **4–7**.

Pinutwindoublin (**1**) is the first A-type-only trimer linked with $(2\alpha \rightarrow O \rightarrow 5,4\alpha \rightarrow 6)$ and $(2\alpha \rightarrow O \rightarrow 7,4\alpha \rightarrow 8)$ bonds. This unprecedented linkage combination is the plausible reason for the observed atropisomeric line-broadening in its NMR spectra, which otherwise is atypical of A-type PACs. Pinuspirotettrin (**2**) represents the first PAC with a heterodimeric framework consisting of a spiro-type dimer connected with an A-type dimer. Also characterized in underivatized form, and exhibiting dentin bioactivity, pinumassohexin (**3**) was elucidated as a hexameric PAC with mixed A+B-type interflavanyl linkages (IFLs), assembled from the known tetramer, peanut procyanidin E,⁸ and the dimer, epicatechin- $(2 \rightarrow O \rightarrow 7,4 \rightarrow 8)$ -*ent*-catechin (**5**),^{8,9} via a $4\beta \rightarrow 6$ bond. Structure elucidation of **1–3** utilized 1D/2D NMR,

ECD, ^{13}C NMR γ -gauche effects, as well as phloroglucinolysis, a recently established toolbox for absolute stereochemical assignments in PACs.⁸

The molecular formula $\text{C}_{45}\text{H}_{34}\text{O}_{18}$ of **1** was determined using the ^{13}C NMR carbon counts and the (+)-HRESIMS ion at m/z 863.1823 $[\text{M} + \text{H}]^+$. Two pairs of characteristic AX-resonances at δ_{H} 3.87 and 4.26 (both d, $J = 4.0$ Hz), as well as δ_{H} 4.22 and 4.87 (both d, $J = 4.3$ Hz), revealed the presence of two doubly linked interflavanyl bonds and, in connection with the molecular formula, indicated the 2A-type trimer nature of **1**. The NMR data (Table S1) showed the characteristic ^1H AMX patterns of the three 1,3,4-trisubstituted aromatic B-, E-, and H-rings. Additionally, a small J coupling (<1 Hz) between III-H-2 and III-H-3 suggested the terminal unit III to be 2,3-*cis* configured (*ent*)-epicatechin. The IFLs were elucidated via HMBC and NOESY data (Figure S1): the presence of $2 \rightarrow \text{O} \rightarrow 7/4 \rightarrow 8$ linkages between units II and III was assigned by the HMBC cross-peaks from both II-H-4 (δ_{H} 4.87) and III-H-2 (δ_{H} 4.96) to III-C-9 (δ_{C} 152.4). The NOESY correlations from II-H-8 to II-H-2' and II-H-6', and from I-H-2' to II-H-4 and III-H-2 indicated that $2 \rightarrow \text{O} \rightarrow 5/4 \rightarrow 6$ bonds connected units I and II. This established the planar structure of **1**.

The absolute configuration of **1** was gleaned from ECD and NOESY data (Figure S1). Due to a high-amplitude negative Cotton effect (CE) in the diagnostic region 220~240 nm (Figure 2A), the C-4 aryl functionalities in both units II and III were determined to be α -configured.¹⁰⁻¹² The absolute configuration of C-4 in units I and II were, thus, assigned as *S* and *R*, respectively (note the change in Cahn–Ingold–Prelog priorities due to different connections, causing different stereodescriptors for spatially identical configurations at both C-4).¹² Taking into account the 2,4-*cis* configuration in A-type PACs,¹³ units I/II and II/III had to be doubly connected via ($2\alpha \rightarrow \text{O} \rightarrow 5,4\alpha \rightarrow 6$) and ($2\alpha \rightarrow \text{O} \rightarrow 7,4\alpha \rightarrow 8$) IFLs, respectively.

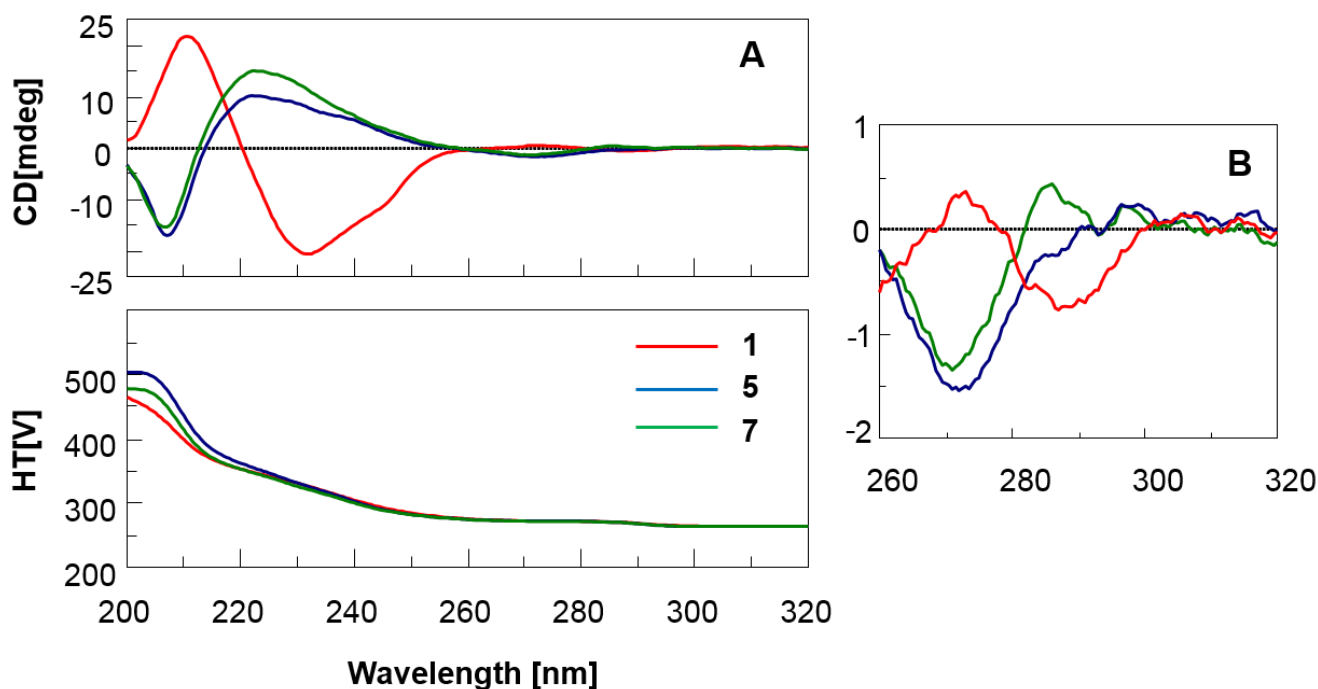


Figure 2. Full ECD spectra (A) of **1**, **5**, and **7** with expansions for the diagnostic range 260–320 nm (B).

A NOESY correlation between II-H-3 and III-H-6 indicated a 3,4-*trans* configuration in the F-ring, thus II-C-3 was *S*-configured.¹¹ Comparison of the tendency of ECD curves of **1** in the diagnostic region 280~300 nm with those of procyanidin A2 (**5**)⁸ and procyanidin A5 (**7**)⁸ revealed that **1** is closely mirror symmetric to **7** (Figure 2B). Thus, the partial structures of units II and III in **1** were assigned to be enantiomeric to those in **7**. This was consistent with the *R*-configuration of III-C-2 deduced from the negative CE at 280~300 nm,^{10,11} and the NOESY correlation of II-H-4 and III-H-6'. Finally, I-H-3 had to be β -

oriented based on NOESY correlations between I-H-3 and both III-H-2 and III-H-6'. Accordingly, **1** was assigned as *ent*-epicatechin-(2 α -O \rightarrow 5,4 α -6)-*ent*-epicatechin-(2 α -O \rightarrow 7,4 α -8)-epicatechin.

This makes **1** the first reported double A-type trimer with an unusual (2 α -O \rightarrow 5,4 α -6) IFL. Restricted rotation along the C-4 aryl (*sp*³-*sp*²) carbon-carbon bond is otherwise only typical for B-type PACs, thereby giving rise to atropisomerism and often severe NMR line broadening at ambient temperature. In contrast, A-type PACs, with two IFLs, generally do not exhibit atropisomerism due to the rigidity of the double linkage.^{6,14,15} Improving ¹H NMR lineshapes of **1** required acquisition at low temperature (255 K; Figure 3). The unexpected dynamic peak broadening of **1** despite its two double linkages indicated that the combination of (2 α -O \rightarrow 5,4 α -6) and (2 α -O \rightarrow 7,4 α -8) IFLs poses sufficient steric hindrance for restricted rotation between rings B and H to generate observable atropisomers, thus leading to NMR line-broadening.

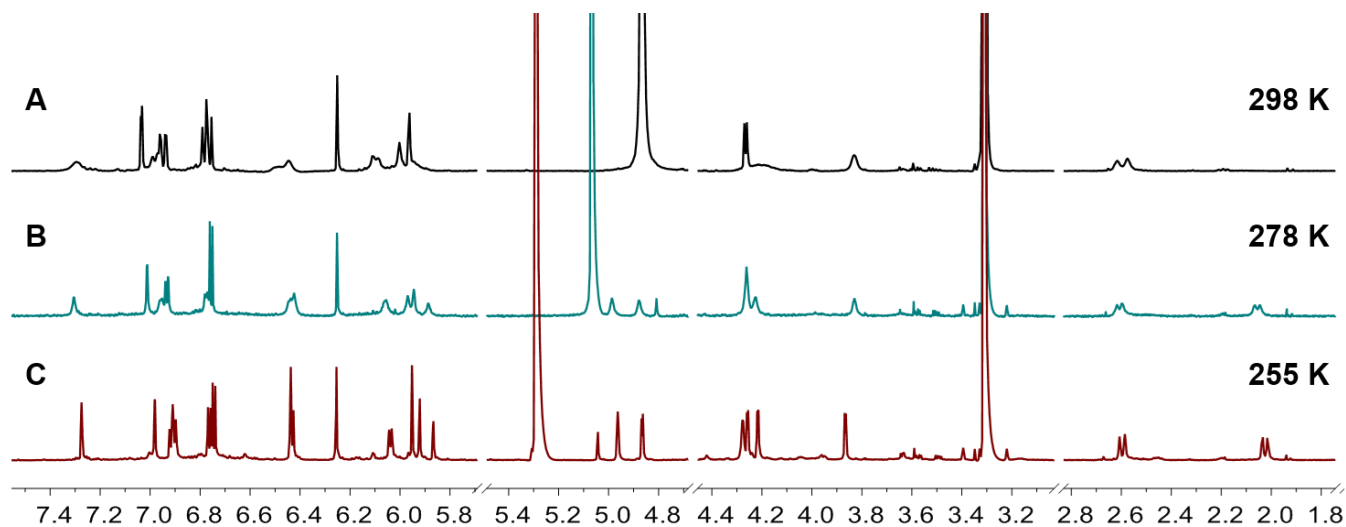
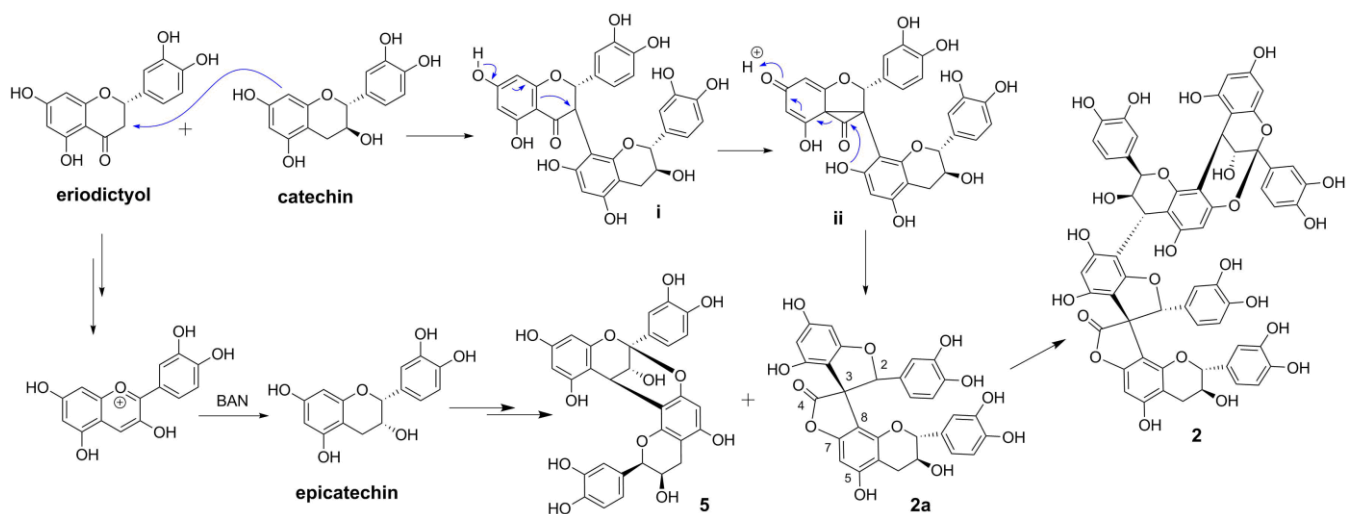


Figure 3. The ¹H NMR spectra of **1** acquired in CD₃OD under the following conditions: A) 298 K at 400 MHz, NS = 64; B) 278 K at 800 MHz, NS = 64; C) 255 K at 800 MHz, NS = 128.

PAC tetramer **2** exhibited a molecular ion at *m/z* 1149.2291 [M + H]⁺ in the (+)-HRESIMS, corresponding to a molecular formula C₆₀H₄₄O₂₄, as supported by the ¹³C NMR data. Lower temperature (255 K) was applied during the 1D and 2D NMR experiments to overcome line broadening due to atropisomerism (Figure S10).^{6,14,16} Analysis of the ¹H NMR spectrum showed four AMX spin systems, corresponding to four 1,3,4-trisubstituted aromatic rings (B/E/H/K). Three singlets at δ_{H} 5.90, 5.96, and 6.16, as well as two *meta*-coupled doublets at δ_{H} 6.02 and 6.03 (*J* = 2.3 Hz) showed the presence of aromatic rings J, G, D, and A, and further confirmed the tetrameric nature of **2**. Two sequential spin systems (δ_{H} 3.70 and 4.44, both d, *J* = 3.5 Hz; and δ_{H} 5.30, 3.95, and 4.47, each brs) that assigned by the COSY data (Figure 4A), indicated the presence of one double (A-type) and one single (B-type) IFL of **2**. Units II and IV were identified as (*ent*)-epicatechin and (*ent*)-catechin, respectively, based on the *J*_{2,3} values of ~0 and 6.3 Hz.

Unusual features involved an oxygenated methine (δ_{H} 5.81, s, and δ_{C} 88.2) that showed HMBC correlations with the carbonyl carbon at δ_{C} 177.0 assigned to a γ -lactone, and a spiro carbon resonating at δ_{C} 61.4. Both are characteristic for a spiro-biflavanoid similar to larixinol.^{17,18} Linkages between the four units were further elucidated by HMBC and NOESY (Figure 4). Units I and II were recognized as being connected by double (2 \rightarrow O \rightarrow 7/4 \rightarrow 8) IFLs based on the I-H-4/II-H-2 NOESY correlation, as well as shift of II-C-8 (δ_{C} 106.3).^{7,19} The presence of a 4 \rightarrow 8 linkage between units II and III was deduced from the cross-peaks between II-H-2 and both III-H-2' and III-H-6' in NOESY spectrum. The spiro-biflavanoid arrangement of units III and IV was corroborated by the HMBC correlations from III-H-2 to III-C-3, III-C-4, III-C-10, III-C-2', III-C-6', and IV-C-8; from IV-H-2 to IV-C-9; and from IV-H-6 to IV-C-5 and IV-C-7. Thus, the planar structure of **2** had to be the first tetrameric spiro-PAC, consisting of one A-type and

one spiro-type dimer. Analysis of its ECD spectrum showed a high-amplitude positive Cotton effect in



Scheme 1. Proposed biosynthetic pathway for the formation of the spiro element in PAC tetramer **2**.

the region 220~240 nm (Figure S2), characteristic for β -substituted flavan-3-ol moieties,¹⁰⁻¹² confirming the absolute configuration of the spiro center III-C-3 as being *S*.¹⁸ The absolute configurations of the C-4 centers in both units I and II were thus assigned as *R*-configured. I-C-2 was *S*-configured based on the inherent 2,4-*cis* configuration in A-type PACs.¹³ A NOESY correlation between I-H-3 and II-H-6 indicated H-3 and H-4 in the C-ring to be *trans*, thus I-C-3 was *R*-configured.¹¹ The upfield shift of II-C-2 (δ_{C} 78.7) suggested a 2,4-*trans*-configuration in the F-ring based on the γ -gauche effect.^{20,21} Unit II was, therefore, epicatechin (2*R*, 3*R*), which was confirmed by the NOESY correlations between II-H-2/III-H-2' and III-H-6'. NOESY correlations from III-H-2 to IV-H-3, IV-H-2', and IV-H-6' assigned III-C-2 as *R*-configured, which determined the terminal unit IV as catechin (2*R*, 3*S*). In conclusion, the structure of **2**, was assigned unambiguously as shown and named as pinuspirotetrin.

The molecular formula $\text{C}_{90}\text{H}_{68}\text{O}_{36}$ gleaned from (+)-HRESIMS and ^{13}C NMR carbon counts identified **3** as a hexamer with 3A+2B IFLs. The close resemblance of the ^1H and ^{13}C NMR resonances of units II/IV and III/V, as well as their congruence with reported data of the major tetramer from peanuts, peanut procyanidin E,⁸ suggested this tetramer plus an additional A-type dimer as building blocks of **3**. Its ^1H NMR spectrum revealed three AX-type doublet pairs (δ_{H} 4.13 and 4.47, $J = 3.4$ Hz; δ_{H} 4.17 and 4.38, $J = 3.6$ Hz; and δ_{H} 4.12 and 4.23, $J = 3.6$ Hz), which corroborated the presence of three doubly linked A-type motifs. Similarly, two B-type single bond linkages were assigned by the observed two sets of three coupled methines resonating as broad singlets at δ_{H} 5.27, 4.04, and 4.74 as well as δ_{H} 5.42, 3.89, and 4.78. All three A-type IFLs were assigned as $2\beta \rightarrow \text{O} \rightarrow 7/4\beta \rightarrow 8$ via NOESY correlations (Figure S22) from H-4 (rings C, I, and O) to H-2 (rings F, L, and R), as well as a strongly positive Cotton effect in the region 220~240 nm (Figure S2). The 3-OH functional groups in rings C, I, and O had to be *trans*-oriented relative to H-4 based on the NOESY correlations from H-3 (rings C, I, and O) to H-6 (rings D, J, and P). The two $4\beta \rightarrow 6$ linkages were deduced from the chemical shifts of C-6 (δ_{C} 110.5 in the G-ring, and δ_{C} 111.0 in the M-ring) and ECD evidence. Units II and IV were both elucidated as epicatechin by the singlet signals of II-H-2 and IV-H-2, and the upfield shifted C-2 (δ_{C} 78.7 in F-ring, and δ_{C} 79.9 in the L-ring) to the corresponding carbon in **4** (δ_{C} 81.6).⁸ Phloroglucinolysis⁸ confirmed the absolute stereochemical assignments. Analysis of the reaction products used a combination of chiral HPLC and MS (Figure S24) to verify that **4** and **5** are the basic components of **3**. Collectively, this assigned the structure of pinumassohexin (**3**) unambiguously as [PAC **5**]-($4\beta \rightarrow 6$)-[PAC **5**]-($4\beta \rightarrow 6$)-[PAC **4**].

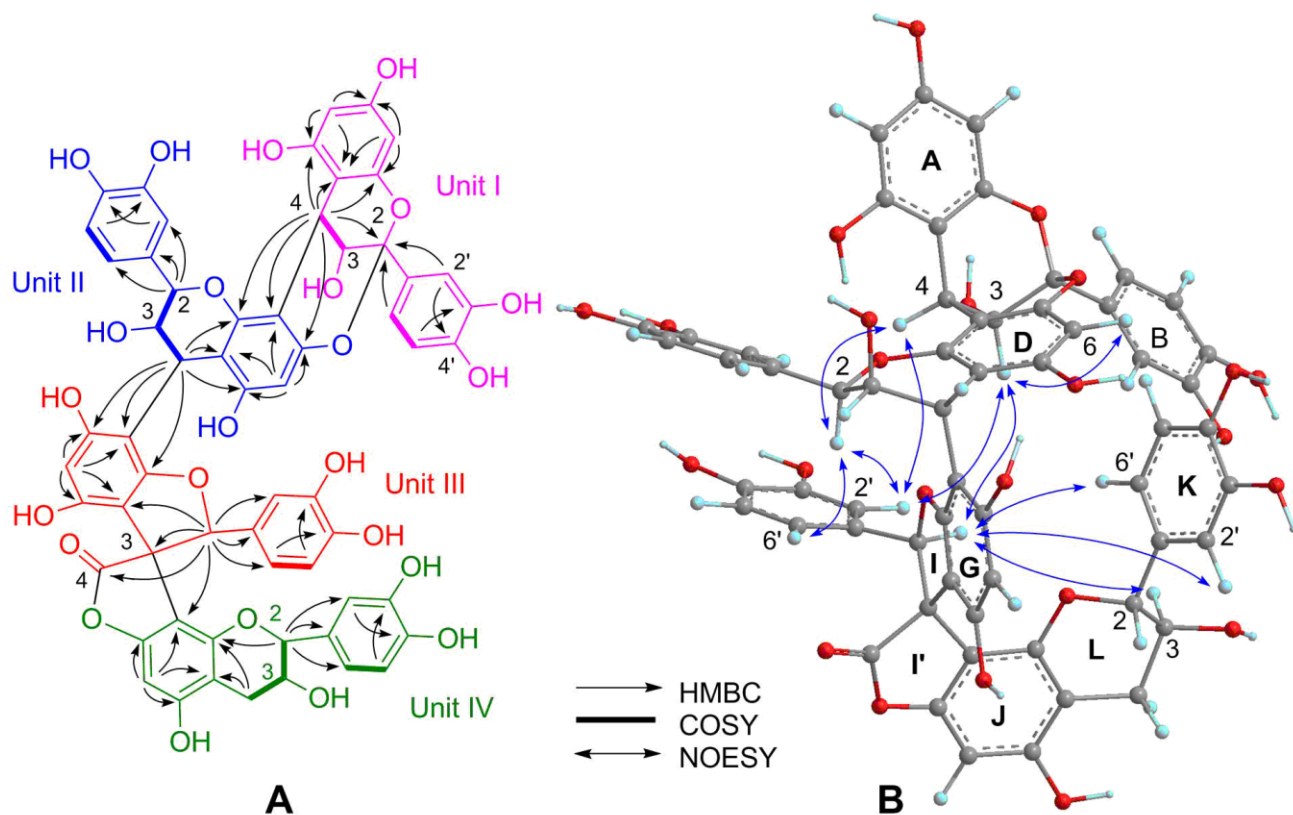


Figure 4. (A) Selected COSY (bold bond), HMBC, and (B) NOESY correlations in **1**.

Pinuspirotetrin (**2**) represents the first heterodimeric framework in any PAC, consisting of a spiro-type dimer (**2a**) and an A-type dimer (**5**). Scheme 1 shows a plausible biosynthetic pathway for **2**, which rationalizes the spiro dimer **2a** as resulting from intermediates (i→ii→**2a**) via oxidative flavanone-flavonol conversion.²²

While all isolates stemmed from a bioactive fraction, only **3** could be evaluated for dentin bioactivity due to limited yields. Hexamer **3** increased the modulus of elasticity of dentin by 4.3-fold, a value between those of A-type dimers (**4–7**) and the most highly potent trimer and tetramers. This further supports the overall hypothesis that medium-size ($n = 3$ and 4) PACs elicit the highest increase in key mechanical properties of dentin. These enhancements to the dentin have promising therapeutic application for the development of novel dental biomaterials. A comprehensive structure and bioactivity relationships of PACs will be reported in due course. While the structural novelties of **1** and **2**, and the unusual size and complexity of **3** did not infer bioactivity in the dentin bioassays, they contribute valuable SAR information and expand the 3D chemical diversity space of condensed tannins.

ASSOCIATED CONTENT

The Supporting Information and Experimental details, ECD spectra of compounds **2** and **3**, 1D and 2D NMR, and HRESIMS of compounds **1–3**; and phloroglucinolysis of **3** were appended in the end.

The raw NMR data (FIDs) are made available at: [DOI:10.7910/DVN/CI2ODS](https://doi.org/10.7910/DVN/CI2ODS).

AUTHOR INFORMATION

Corresponding Author

*Shao-Nong Chen

E-mail: sc4sa@uic.edu.

Notes

The authors declare no competing financial interest.

ACKNOWLEDGMENT

This research was supported by grant R01 DE021040 from NIDCR/NIH. We are thankful to Drs. Joseph Ray, David Lankin, and Benjamin Ramirez for NMR discussions and support. The construction of the UIC Center for Structural Biology (CSB) facility and 800 MHz NMR instrument purchase was generously funded by NIGMS grant # P41 GM068944 awarded to Dr. Peter Gettins (PI).

REFERENCES

- (1) Li, W. G.; Zhang, X. Y.; Wu, Y. J.; Tian, X. Anti-inflammatory effect and mechanism of proanthocyanidins from grape seeds. *Acta Pharmacol. Sin.* **2001**, *22*, 1117–1120.
- (2) Anderson, R. A.; Broadhurst, C. L.; Polansky, M. M.; Schmidt, W. F.; Khan, A.; Flanagan, V. P.; Schoene, N. W.; Graves, D. J. Isolation and characterization of polyphenol type-A polymers from cinnamon with insulin-like biological activity. *J. Agric. Food Chem.* **2004**, *52*, 65–70.
- (3) Mandel, S.; Youdim, M. B. H. Catechin polyphenols: neurodegeneration and neuroprotection in neurodegenerative diseases. *Free Radical Biol. Med.* **2004**, *37*, 304–317.
- (4) Kim, Y. J.; Park, H. J.; Yoon, S. H.; Kim, M. J.; Leem, K. H.; Chung, J. H.; Kim, H. K. Anticancer effects of oligomeric proanthocyanidins on human colorectal cancer cell line, SNU-C4. *World J. Gastroenterol.* **2005**, *11*, 4674–4678.
- (5) Skerget, M.; Kotnik, P.; Hadolin, M.; Hras, H. R.; Simonic, M.; Knez, Z. Phenols, proanthocyanidins, flavones and flavonols in some plant materials and their antioxidant activities. *Food Chem.* **2005**, *89*, 191–198.
- (6) Nam, J. W.; Phansalkar, R. S.; Lankin, D. C.; Bisson, J.; McAlpine, J. B.; Leme, A. A.; Vidal, C. M. P.; Ramirez, B.; Niemitz, M.; Bedran-Russo, A.; Chen, S. N.; Pauli, G. F. Subtle chemical shifts explain the NMR fingerprints of oligomeric proanthocyanidins with high dentin biomodification potency. *J. Org. Chem.* **2015**, *80*, 7495–7507.
- (7) Nam, J. W.; Phansalkar, R. S.; Lankin, D. C.; McAlpine, J. B.; Leme-Kraus, A. A.; Vidal, C. M. P.; Gan, L. S.; Bedran-Russo, A.; Chen, S. N.; Pauli, G. F. Absolute configuration of native oligomeric proanthocyanidins with dentin biomodification potency. *J. Org. Chem.* **2017**, *82*, 1316–1329.
- (8) Zhou, B. Y.; Alania, M.; Reis, R.; Phansalkar, J. W.; Nam, J.; McAlpine, J.; Chen, S. N.; Bedran-Russo, G.; Pauli, G. F. Tri- and Tetrameric Proanthocyanidins with Dentin Bioactivities from *Pinus massoniana*. ChemRxiv <https://figshare.com/s/bb3c881919116125ed65>.
- (9) Jacques, D.; Haslam, E.; Bedford, G. R.; Greatbanks, D. Plant proanthocyanidins. Part II. Proanthocyanidin-A2 and its derivatives. *J. Chem. Soc., Perkin Trans. 1* **1974**, 2663–2671.
- (10) Botha, J. J.; Young, D. A.; Ferreira, D.; Roux, D. G. Synthesis of condensed tannins. Part 1. Stereoselective and stereospecific syntheses of optically pure 4-arylflavan-3-ols, and assessment of their absolute stereochemistry at C-4 by means of circular dichroism. *J. Chem. Soc., Perkin Trans. 1* **1981**, 1213–1219.
- (11) Kolodziej, H.; Sakar, M. K.; Burger, J. F.; Engelshove, R.; Ferreira, D. A-type proanthocyanidins from *Prunus spinosa*. *Phytochemistry* **1991**, *30*, 2041–2047.
- (12) Slade, D.; Ferreira, D.; Marais, J. P. Circular dichroism, a powerful tool for the assessment of absolute configuration of flavonoids. *Phytochemistry* **2005**, *66*, 2177–2215.
- (13) Bilia, A.; Morelli, I.; Hamburger, M.; Hostetmann, K. Flavans and A-type proanthocyanidins from *Prunus prostrata*. *Phytochemistry* **1996**, *43*, 887–892.
- (14) Fletcher, A. C.; Porter, L. J.; Haslam, E.; Gupta, R. K. Plant proanthocyanidins. Part 3. Conformational and configurational studies of natural procyanidins. *J. Chem. Soc., Perkin Trans. 1* **1977**, 1628–1637.
- (15) Dudek, M. K.; Glinski, V. B.; Davey, M. H.; Sliva, D.; Kazmierski, S.; Glinski, J. A. Trimeric and tetrameric A-type procyanidins from peanut skins. *J. Nat. Prod.* **2017**, *80*, 415–426.

- (16) Killday, K. B.; Davey, M. H.; Glinski, J. A.; Duan, P. G.; Veluri, R.; Proni, G.; Daugherty, F. J.; Tempesta, M. S. Bioactive A-type proanthocyanidins from *Cinnamomum cassia*. *J. Nat. Prod.* **2011**, *74*, 1833–1841.
- (17) Shen, Z. B.; Falshaw, C. P.; Haslam, E.; Begley, M. J. A novel spiro-biflavonoid from *Larix gmelini*. *J. Chem. Soc. Chem. Commun.* **1985**, 1135–1137.
- (18) Wada, S.; Hitomi, T.; Tanaka, R. Phenolic compounds isolated from the bark of *Abies sachalinensis*. *Helv. Chim. Acta* **2009**, *92*, 1610–1620.
- (19) Lou, H. X.; Yamazaki, Y.; Sasaki, T.; Uchida, M.; Tanaka, H.; Oka, S. A-type proanthocyanidins from peanut skins. *Phytochemistry* **1999**, *51*, 297–308.
- (20) Cai, Y.; Evans, F. J.; Roberts, M. F.; Phillipson, J. D.; Zenk, M. H.; Gleba, Y. Y. Polyphenolic compounds from *Croton lechleri*. *Phytochemistry* **1991**, *30*, 2033–2040.
- (21) Lokman Khan, M.; Haslam, E.; Williamson, M. P. Structure and conformation of the procyanidin B-2 dimer. *Magn. Reson. Chem.* **1997**, *35*, 854–858.
- (22) Shen, Z.; Haslam, E.; Falshaw, C. P.; Begley, M. J. Procyanidins and polyphenols of *Larix gmelini* bark. *Phytochemistry* **1986**, *25*, 2629–2635.

Rare A-Type, New Spiro-Type, and Highly Oligomeric Proanthocyanidins from *Pinus massoniana*

Bin Zhou^{1,†}, Yvette Alania^{3,4}, Mariana C. Reis^{3,4}, James B. McAlpine^{1,2} Ana K. Bedran-Russo^{2,3,4}, Guido F. Pauli^{1,2}, and Shao-Nong Chen^{1,2,*}

¹Department of Pharmaceutical Sciences and ²Program for Collaborative Research in the Pharmaceutical Sciences (PCRPS), College of Pharmacy, ³Department of Restorative Dentistry, College of Dentistry, University of Illinois at Chicago, Chicago, Illinois 60612, USA; ⁴Department of General Dental Sciences, School of Dentistry, Marquette University, Milwaukee, Wisconsin 53233, USA.

†Present Address: State Key Laboratory of Drug Research, Shanghai Institute of Materia Medica, Chinese Academy of Sciences, 555 Zuchongzhi Road, Shanghai 201203, People's Republic of China

Table of Contents

Table S1. ^1H (800 MHz) and ^{13}C NMR (100 MHz) data of 1–3 in CD_3OD	1
Figure S1. (A) Selected COSY (bold bonds), HMBC, and (B) NOESY correlations (arrows) in 1	3
Figure S2. The ECD spectra of 2 and 3	4
■ EXPERIMENTAL SECTION	5
General Experimental Procedures	5
Plant Material	5
Extraction and Isolation of PACs	5
Phloroglucinolysis	6
Compounds properties	6
Figure S3. ^1H NMR spectrum of 1 in CD_3OD (800 MHz, 255 K).	7
Figure S4. ^{13}C NMR spectrum of 1 in CD_3OD (100 MHz, 255 K).	7
Figure S5. HSQC spectrum of 1 in CD_3OD (255 K).	8
Figure S6. HMBC spectrum of 1 in CD_3OD (255 K).	8
Figure S7. NOESY spectrum of 1 in CD_3OD (255 K).....	9
Figure S8. (+)-HRESIMS spectrum of 1	9
Figure S9. ^1H NMR spectrum of 2 in CD_3OD (800 MHz, 255 K).	10
Figure S10. Comparison of the ^1H NMR spectra of 2 in CD_3OD at 278 K and 255 K (800 MHz).....	10
Figure S11. ^{13}C NMR spectrum of 2 in CD_3OD (100 MHz, 255 K).	11
Figure S12. ^1H - ^1H COSY spectrum of 2 in CD_3OD (255 K).....	11
Figure S13. HSQC spectrum of 2 in CD_3OD (255 K).	12
Figure S14. HMBC spectrum of 2 in CD_3OD (255 K).	12
Figure S15. NOESY spectrum of 2 in CD_3OD (255 K).....	13
Figure S16. (+)-HRESIMS spectrum of 2	13
Figure S17. ^1H NMR spectrum of 3 in CD_3OD (800 MHz, 278 K).....	14
Figure S18. ^{13}C NMR spectrum of 3 in CD_3OD (100 MHz, 278 K).	14
Figure S19. ^1H - ^1H COSY spectrum of 3 in CD_3OD (278 K).....	15
Figure S20. HSQC spectrum of 3 in CD_3OD (278 K).	15

Figure S21. HMBC spectrum of 3 in CD ₃ OD (278 K).	16
Figure S22. NOESY spectrum of 3 in CD ₃ OD (278 K).	17
Figure S23. (+)-HRESIMS spectrum of 3	17
Figure S24. Phloroglucinolysis products of 3 identified by chiral phase HPLC and MS analysis.	18

Table S1. ¹H (800 MHz) and ¹³C NMR (100 MHz) data of **1–3** in CD₃OD.

Unit	Ring	No.	1^a		2^a		3^b		Unit	Ring	No.	3^b	
			¹ H (mult., <i>J</i> in Hz)	¹³ C	¹ H (mult., <i>J</i> in Hz)	¹³ C	¹ H (mult., <i>J</i> in Hz)	¹³ C				¹ H (mult., <i>J</i> in Hz)	¹³ C
I	C	2		100.5		99.9		100.0	V	O	2		100.2
		3	3.87, d (4.0)	65.1	3.70, d (3.5)	67.5	4.13, d (3.4)	68.2			3	4.12, d (3.6)	67.6
		4	4.26, d (4.0)	29.7	4.44, d (3.5)	28.9	4.47, d (3.4)	29.4			4	4.23, d (3.6)	29.6
	A	5		155.2		156.9		157.1		M	5		154.1
		6	5.92, d (1.9)	97.3	6.03, d (2.3)	98.0	6.06, d (2.4)	98.2			6		111.0
		7		157.9		157.9		158.0			7		156.7
		8	5.87, d (1.9)	96.1	6.02, d (2.3)	96.2	6.11, d (2.4)	96.6			8	6.083, s	97.5
		9		154.8		154.1		154.1			9		152.1
		10		105.3		104.4		104.2			10		104.0
		B	1'		131.7		131.9				132.5	N	1'
2'	7.29, d (2.1)		116.1	7.01, d (2.1)	115.2	7.18, d (2.1)	115.5	2'	7.14, d (2.2)	115.5			
3'			145.2		145.0		145.5	3'		145.6			
4'			146.6		146.2		146.6	4'		146.7			
5'	6.76, d (8.2)		115.1	6.71, d (8.2)	115.5	6.84, d (8.2)	115.5	5'	6.82, d (8.3)	115.5			
6'	6.90, dd (8.3, 2.1)	120.3	6.61, dd (8.4, 2.1)	119.4	7.06, dd (8.2, 2.1)	119.7	6'	7.04, dd (8.1, 2.3)	119.8				
II	F	2		101.1	5.30, brs	78.7	5.27, s	78.7	VI	R	2	4.78, d (7.7)	85.1
		3	4.22, d (4.3)	68.7	3.95, brs	72.3	4.04, brs	72.3			3	4.19, m	68.2
		4	4.87, d (4.3)	30.4	4.47, brs	38.1	4.74, brs	38.6			4	2.60, dd (16.2, 8.4)	29.0
	D	5		150.8		157.1		156.4		P	4	3.00, dd (16.2, 5.1)	29.0
		6		108.5	5.96, s	95.8	6.13, s	96.1			5		156.2
		7		153.1		151.9		152.2			6	6.14, s	96.6
		8	6.25, s	97.4		106.3		106.8			7		152.1
		9		154.6		152.7		152.3			8		106.4
		10		105.9		105.0		105.6			9		151.2
		E	1'		131.5		131.5				131.4	Q	10
2'	6.98, d (2.2)		115.4	7.21, d (2.1)	116.6	7.161, d (2.1)	116.2	1'		130.0			
3'			145.5		145.8		145.8	2'	7.00, d (2.1)	115.9			
4'			146.6		146.3		146.2	3'		146.2			
5'	6.74, d (8.1)	115.5	6.80, d (8.2)	115.6	6.80, d (8.2)	115.9	4'		146.9				
6'	6.92, dd (8.1, 2.2)	119.7	7.08, dd (8.2, 2.1)	121.4	6.96, dd (8.2, 2.1)	120.7	5'	6.88, d (8.1)	116.8				
III	I	2	4.96, s	79.7	5.81, s	88.2		100.1	6'	6.92, dd (8.2, 2.1)	121.1		
		3	4.28, m	66.9		61.4	4.17, d (3.6)	68.0					

		4	2.02, dd (17.0, 3.5) 2.60, brd (17.0)	23.6 23.6		177.0	4.38, d (3.6)	29.8
	G	5		156.4		154.2		154.6
		6	5.95, s	95.7	5.90, s	96.6		110.5
		7		151.7		158.2		156.8
		8		105.6		106.0	6.082, s	97.4
		9		152.4		162.2		152.1
		10		101.1		106.1		104.4
	H	1'		132.4		128.5		132.3
		2'	6.43, d (2.2)	113.1	6.41, d (2.2)	113.3	7.162, d (2.2)	115.5
		3'		146.1		145.7		145.6
		4'		145.5		145.8		146.7
		5'	6.43, d (8.1)	115.5	6.63, d (8.3)	115.9	6.83, d (8.3)	115.5
		6'	6.04, dd (8.2, 2.2)	117.6	6.53, dd (8.1, 2.3)	118.3	7.05, dd (8.1, 2.3)	119.7
IV	L	2			4.83, d (6.3)	82.5	5.42, s	79.9
		3			3.97, m	68.7	3.89, brs	72.6
		4			2.68, dd (16.4, 7.2)	27.6	4.78, brs	38.4
	J				2.86, dd (16.4, 5.0)	27.6		
		5				158.1		156.7
		6			6.16, s	91.3	6.11, s	96.6
		7				154.5		151.9
		8				104.0		106.2
		9				152.8		152.6
	K	10				104.8		106.0
		1'				131.64		130.8
		2'			6.80, d (2.1)	114.0	7.20, d (2.1)	117.1
		3'				145.9		145.5
		4'				146.0		146.5
		5'			6.74, d (8.1)	115.8	6.78, d (8.1)	115.9
		6'			6.68, dd (8.2, 2.1)	119.7	6.94, dd (8.2, 2.1)	121.8

Data were acquired at ^a255 K and ^b278 K.

Figure S1. (A) Selected COSY (bold bonds), HMBC, and (B) NOESY correlations (arrows) in **1**.

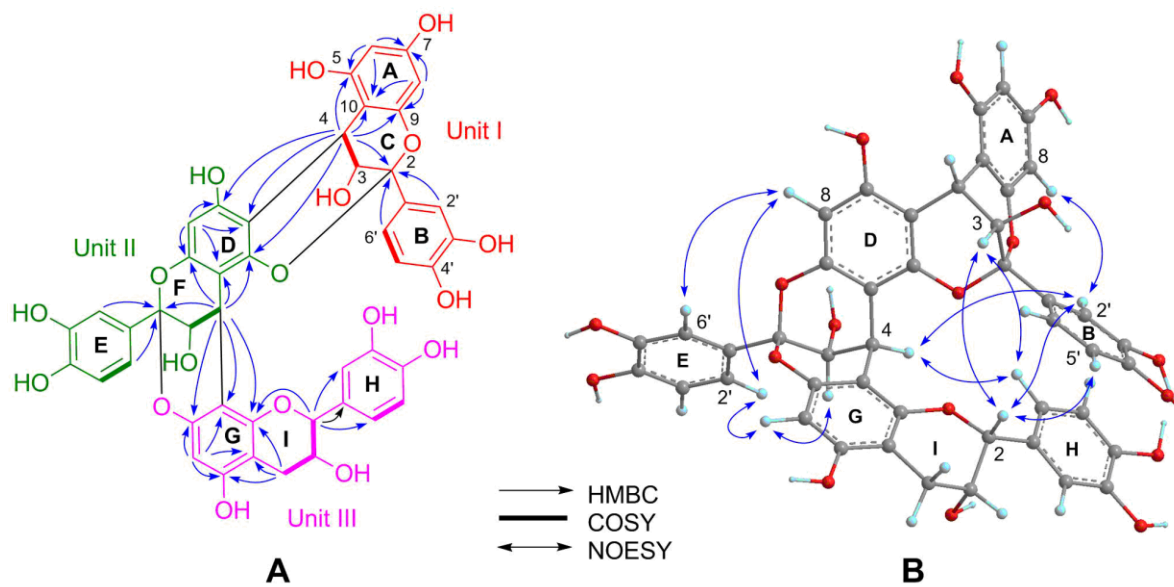
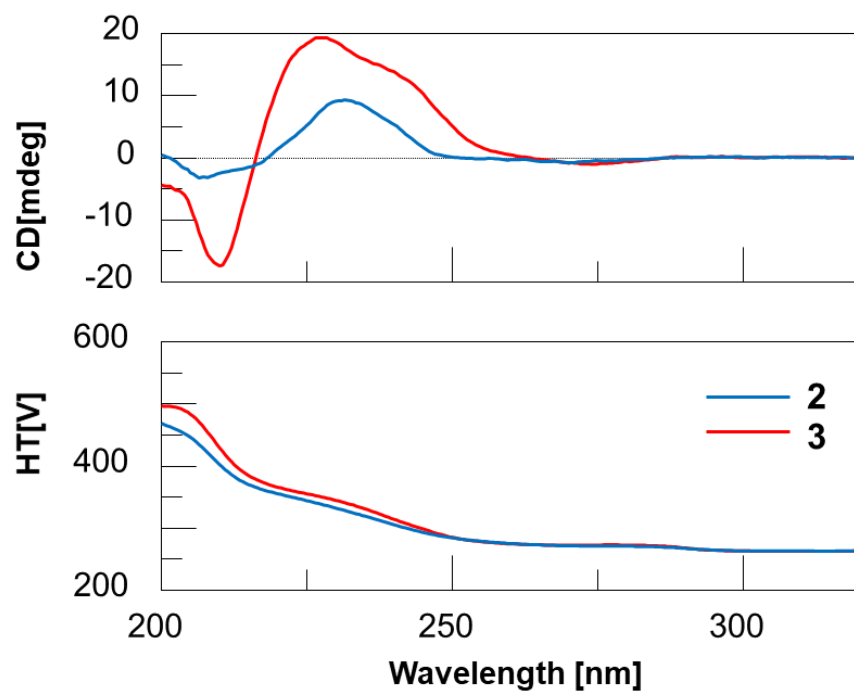


Figure S2. The ECD spectra of **2** and **3**.



■ EXPERIMENTAL SECTION

General Experimental Procedures

HRESIMS measurements were carried out using a Bruker (Billerica, MA, USA) Impact II quadrupole time-of-flight (qTOF-) spectrometer. The ECD spectra were acquired on a JASCO-715 spectrometer. Samples for ECD experiments were prepared in MeOH at ≤ 0.1 mg/mL, and a 0.2 cm path length quartz cuvette was used. All ^1H 1D/2D NMR spectra were acquired at 255 K or 278 K on an 800 MHz Bruker (Billerica, MA, USA) Avance spectrometer equipped with a 5 mm triple resonance inverse TCI RT probe. The ^{13}C NMR experiments of all compounds were performed on a JEOL (JEOL Resonance, Peabody, MA, USA) ECZ 400 MHz spectrometer. Silica gel (230–400 mesh) was used for column chromatography. C_{18} reversed-phase (RP-18) silica gel (20–45 μm , MACHEREY-NAGEL, Bethlehem, PA, USA) and Sephadex LH-20 gel (Amersham Biosciences) were used for column chromatography. Pre-coated silica gel GF₂₅₄ plates (MACHEREY-NAGEL, Bethlehem, PA, USA) were used for TLC monitoring. Semi-preparative HPLC was performed on a Shimadzu HPLC (Kyoto, Japan) connected to a PDA detector (Shimadzu, model SPD-20A) and equipped with a YMC-Pack ODS-AQ (250 \times 10 mm, S -5 μm , 120 Å; YMC America, Allentown, USA) or Chiralpak IA (250 \times 10.0 mm, S -5 μm ; Chiral Technologies, West Chester, PA, USA) column. All solvents were of analytical grade from Fisher Scientific (Hanover Park, IL, USA) or Sigma-Aldrich (St. Louis, MO, USA).

Plant Material

Extract powder of the inner bark of *Pinus massoniana* was purchased from Xi'an Chukang Biotechnology in China in 2012 (No. PB120212).

Extraction and Isolation of PACs

12 g of enriched tri- and tetrameric proanthocyanidins, separated into 6.5 g of fraction A and 5.6 g of fraction B, were prepared from 200 g pine bark extract by centrifugal partition chromatography (CPC) as described previously.¹ Both fractions A and B were chromatographed on a Sephadex LH-20 column (ethanol), affording six (A1–A6) and seven subfractions (B1–B7), respectively. Fraction B5 (800 mg) was separated over a RP-18 silica gel column (MeOH/H₂O, 20–80%), and the two major subfractions B5b and B5c were then purified via semi-preparative HPLC (18% ACN in 0.1% formic acid H₂O, 2.5 mL/min) to afford **1** (0.7 mg) and **2** (0.8 mg).

Compound **3** (20 mg) was purified from fraction B7 by semi-preparative HPLC (20% ACN in 0.1% formic acid H₂O, 2.5 mL/min) after enrichment via a RP-18 silica gel column.

Phloroglucinolysis

Phloroglucinolysis was performed as described previously² to corroborate the absolute configuration of **3**. The identity of the reaction products was confirmed by chiral HPLC and MS analysis (Figure S24).

Compounds properties

Pinutwindoublin (**1**): *ent*-epicatechin-(2 α →O→5,4 α →6)-*ent*-epicatechin-(2 α →O→7,4 α →8)-epicatechin: light brown, amorphous solid; ECD (MeOH) λ_{\max} ($\Delta\epsilon$) 211 (+21.6), 232 (−20.8), 287 (−0.8) nm; ¹H and ¹³C NMR (CD₃OD, 255K), see Table 1, (+)-HRESIMS [M + H]⁺ *m/z* 863.1823 (calcd for C₄₅H₃₅O₁₈, 863.1818).

Pinuspirotetrin (**2**): Light brown, amorphous solid; ECD (MeOH) λ_{\max} ($\Delta\epsilon$) 207 (−3.2), 232 (+9.4), 270 (−0.8); ¹³C NNMR (CD₃OD, 255K), see Table 2; (+)-HRESIMS [M + H]⁺ *m/z* 1149.2291 (calcd for C₆₀H₄₅O₂₄, 1149.2295).

Pinumassohexin (**3**): epicatechin-(2 β →O→7,4 β →8)-epicatechin-(4 β →6)-epicatechin-(2 β →O→7,4 β →8)-epicatechin-(2 β →O→7,4 β →8)-epicatechin-(4 β →6)-catechin: light brown, amorphous solid; ECD (MeOH) λ_{\max} ($\Delta\epsilon$) 210 (−17.3), 228 (+19.3), 274 (−1.0); ¹H and ¹³C NNMR (CD₃OD, 278K), see Table 2; (+)-HRESIMS [M + H]⁺ *m/z* 1725.3589 (calcd for C₉₀H₆₉O₃₆, 1725.3563).

References

1. Phansalkar, R. S.; Nam, J. W.; Chen, S. N.; McAlpine, J. B.; Leme, A. A.; Aydin, B.; Bedran-Russo, A. K.; Pauli, G. F. Centrifugal partition chromatography enables selective enrichment of trimeric and tetrameric proanthocyanidins for biomaterial development. *J. Chromatogr. A* **2018**, *1535*, 55–62.
2. Zhou, B. Y Alania, M Reis, R. Phansalkar, JW Nam, J McAlpine, SN Chen, A Bedran-Russo, G Pauli. Tri- and Tetrameric Proanthocyanidins with Dentin Bioactivities from *Pinus massoniana*. ChemRxiv <https://figshare.com/s/bb3c881919116125ed65>.

Figure S3. ^1H NMR spectrum of **1** in CD_3OD (800 MHz, 255 K).

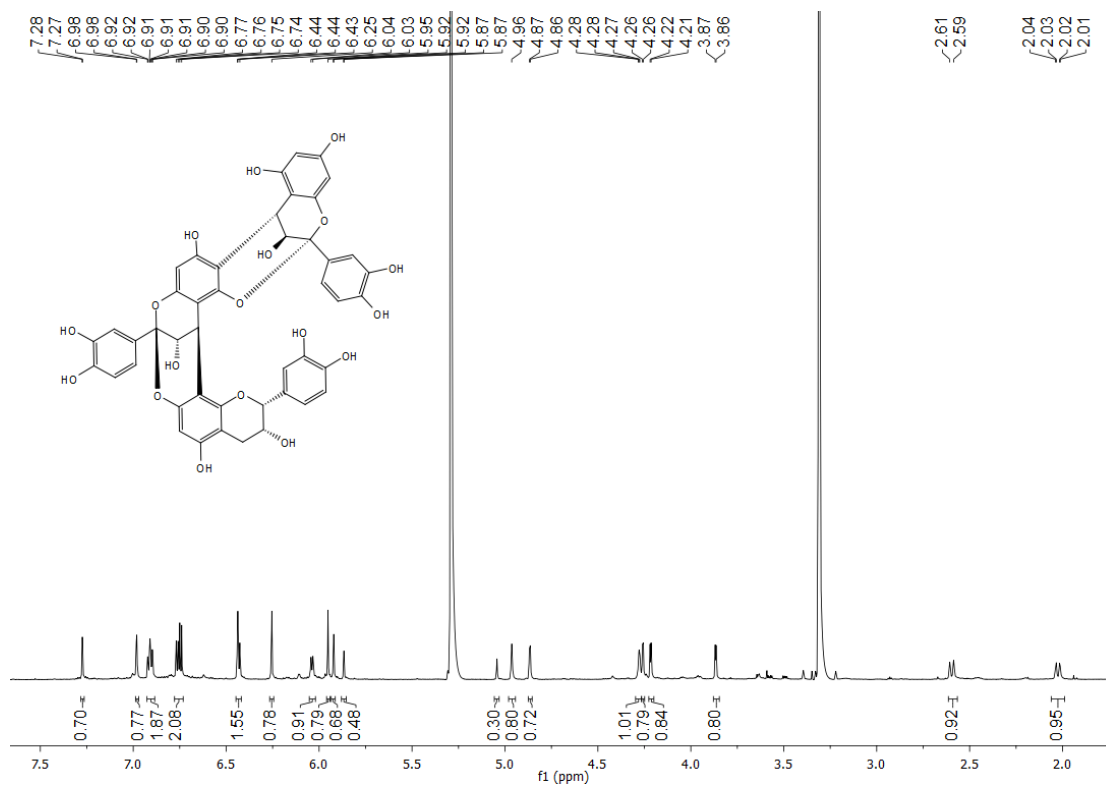


Figure S4. ^{13}C NMR spectrum of **1** in CD_3OD (100 MHz, 255 K).

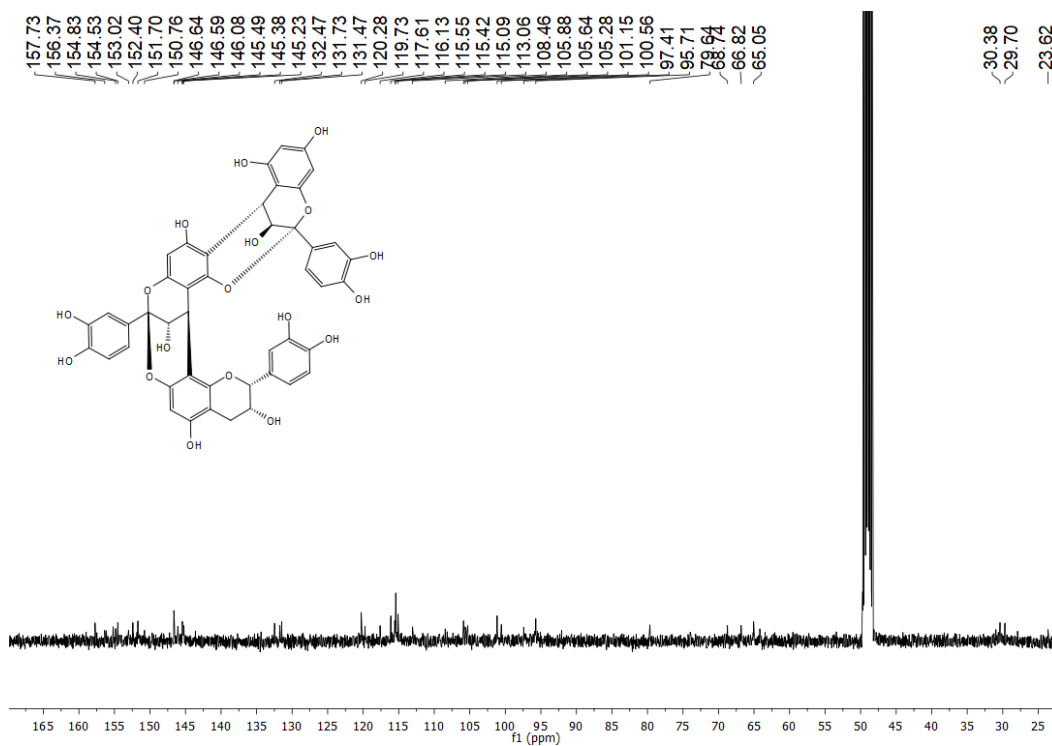


Figure S5. HSQC spectrum of **1** in CD₃OD (255 K).

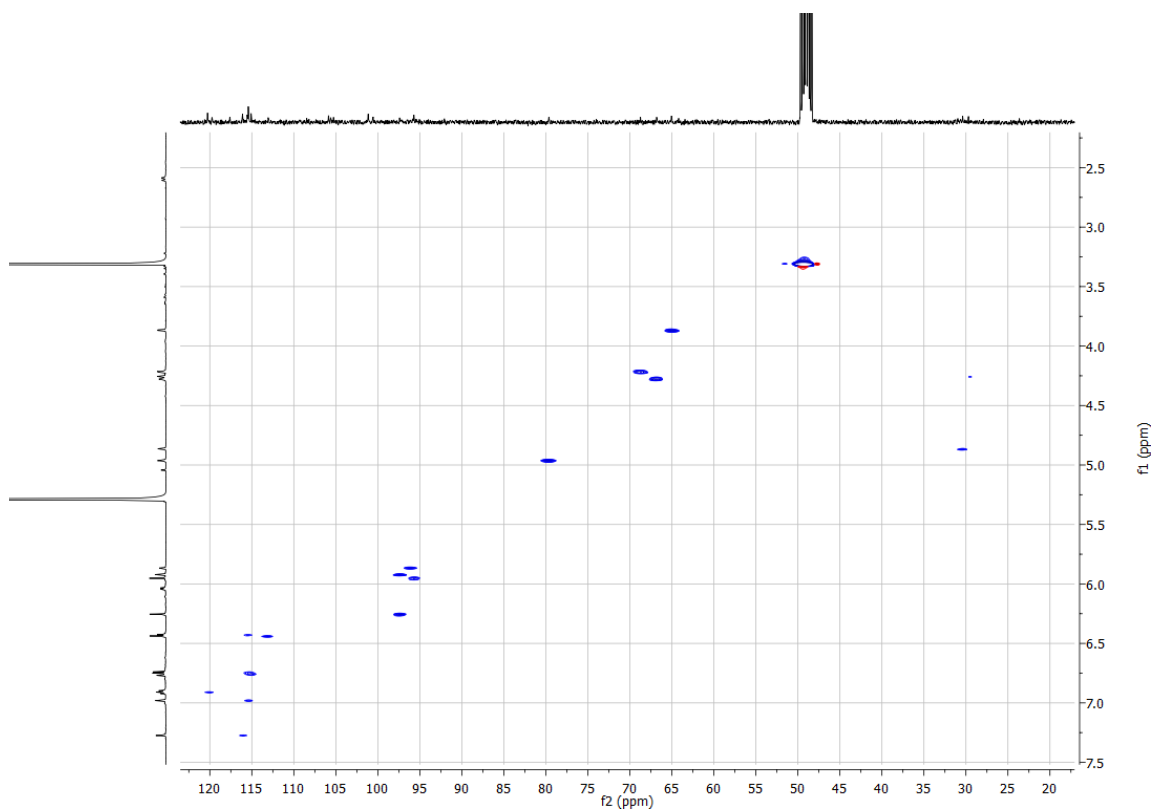


Figure S6. HMBC spectrum of **1** in CD₃OD (255 K).

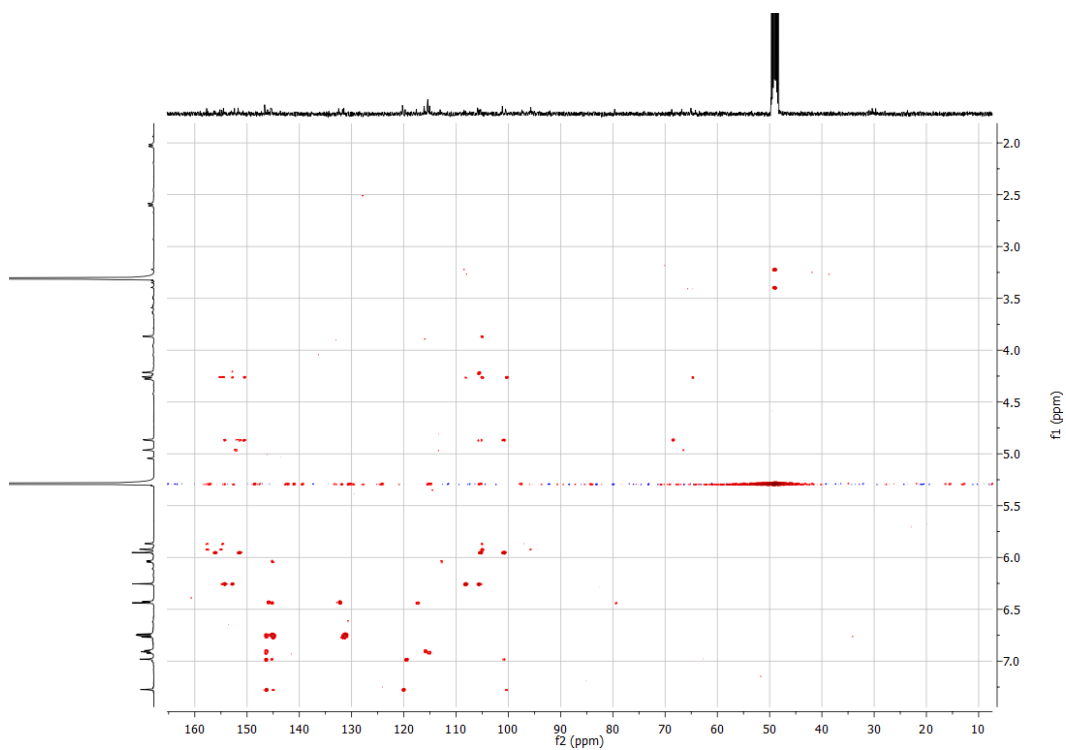


Figure S7. NOESY spectrum of **1** in CD₃OD (255 K).

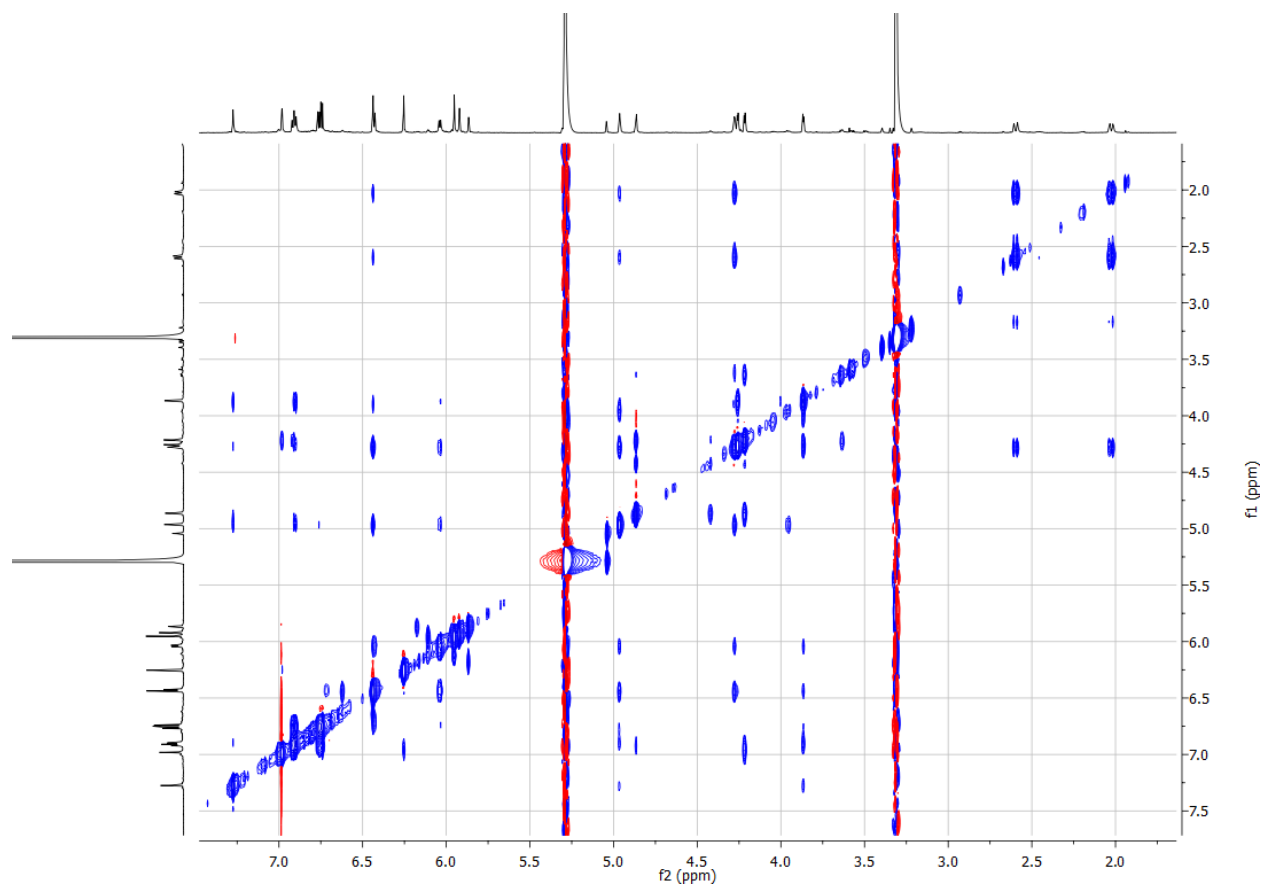


Figure S8. (+)-HRESIMS spectrum of **1**.

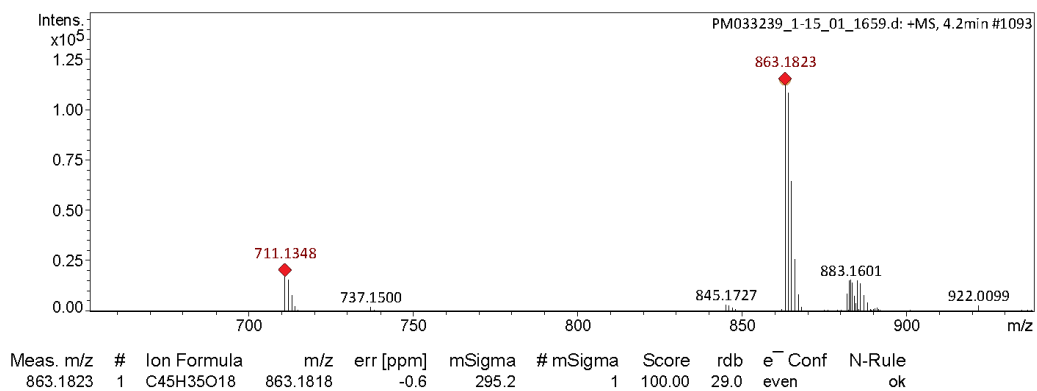


Figure S9. ^1H NMR spectrum of **2** in CD_3OD (800 MHz, 255 K).

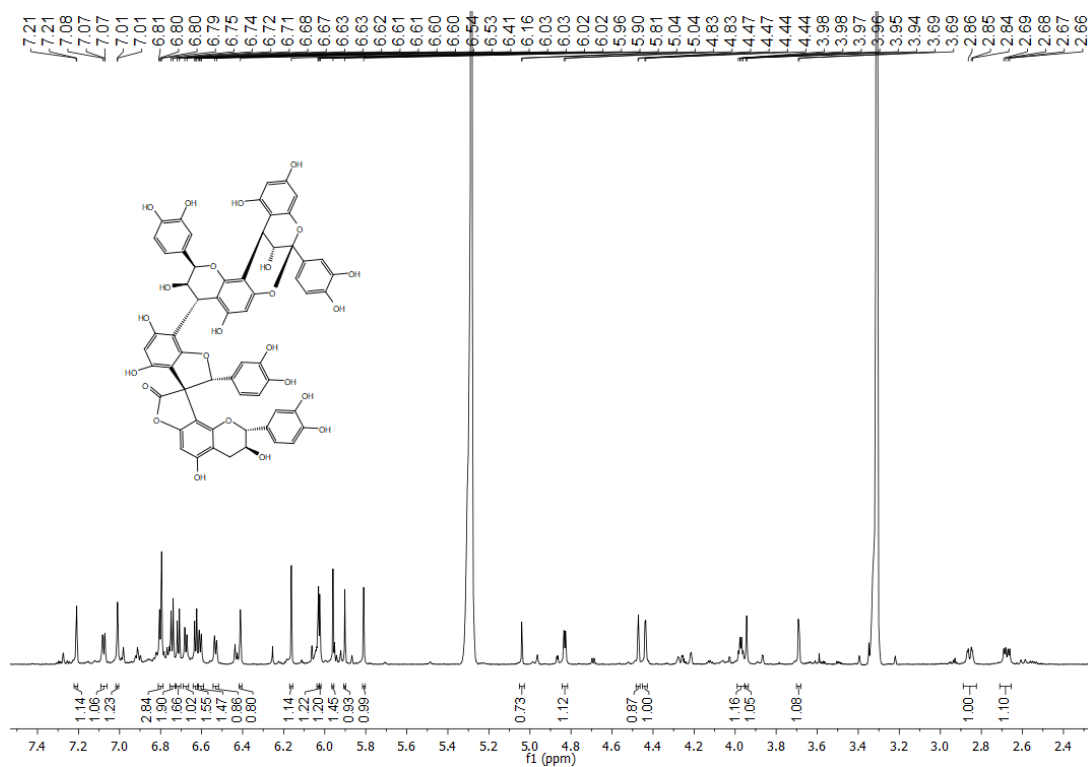


Figure S10. Comparison of the ^1H NMR spectra of **2** in CD_3OD at 278 K and 255 K (800 MHz).

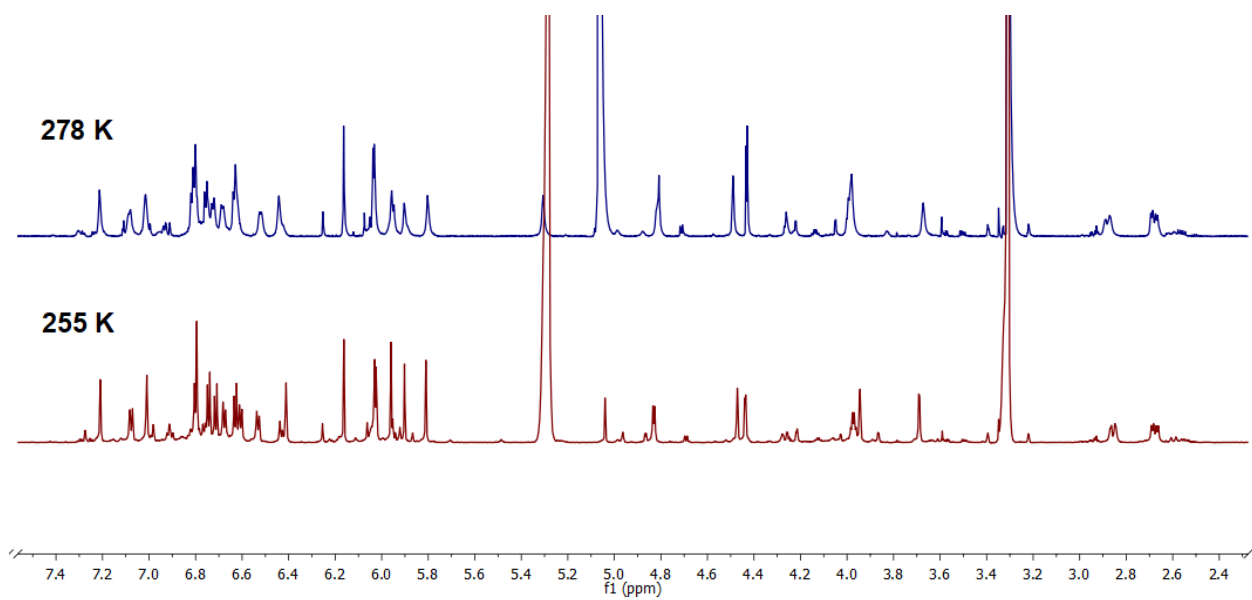


Figure S11. ^{13}C NMR spectrum of **2** in CD_3OD (100 MHz, 255 K).

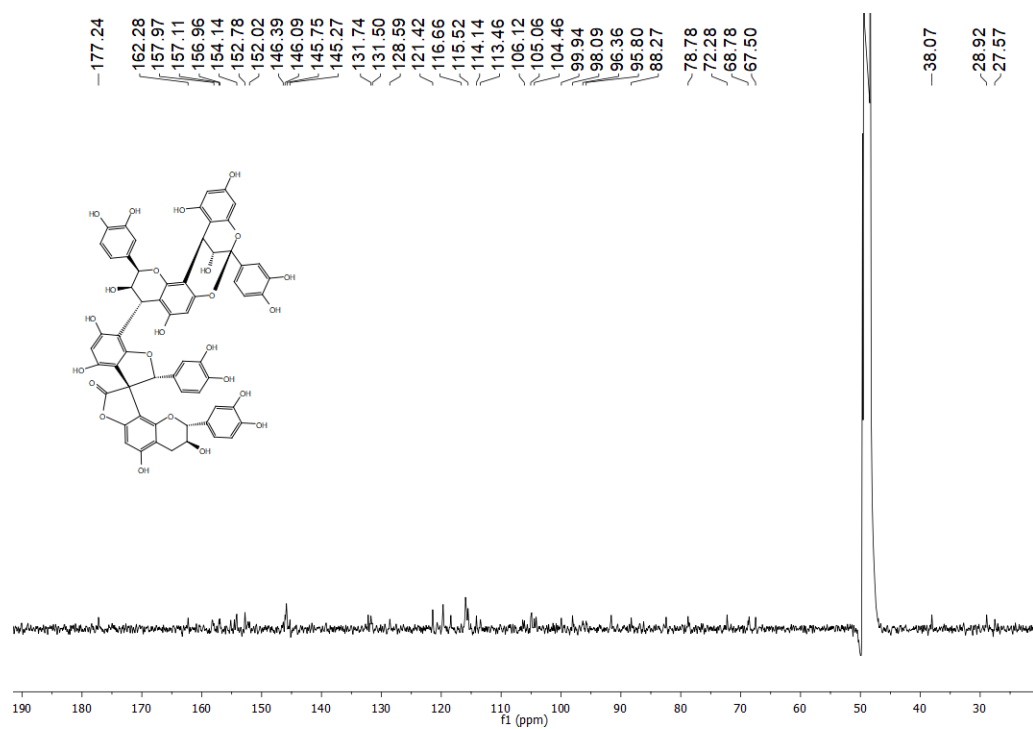


Figure S12. ^1H - ^1H COSY spectrum of **2** in CD_3OD (255 K).

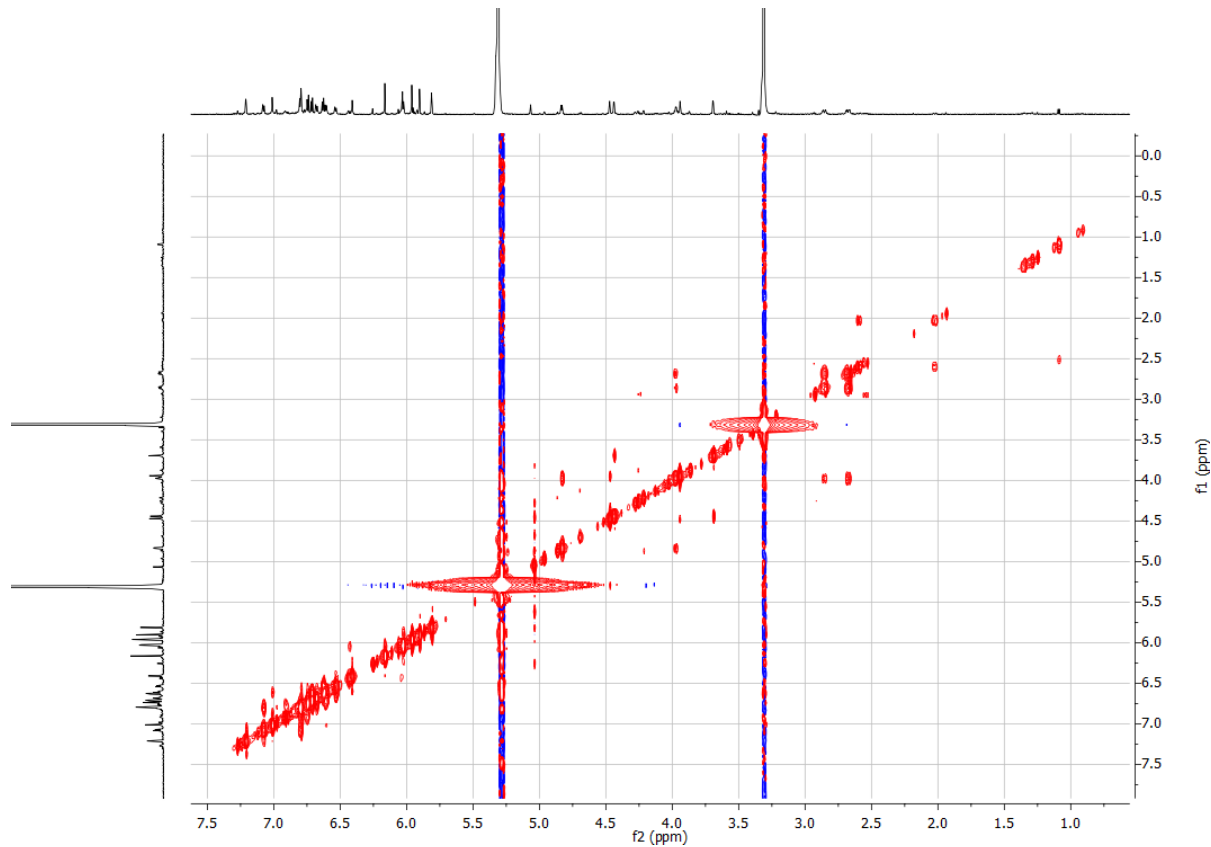


Figure S13. HSQC spectrum of **2** in CD₃OD (255 K).

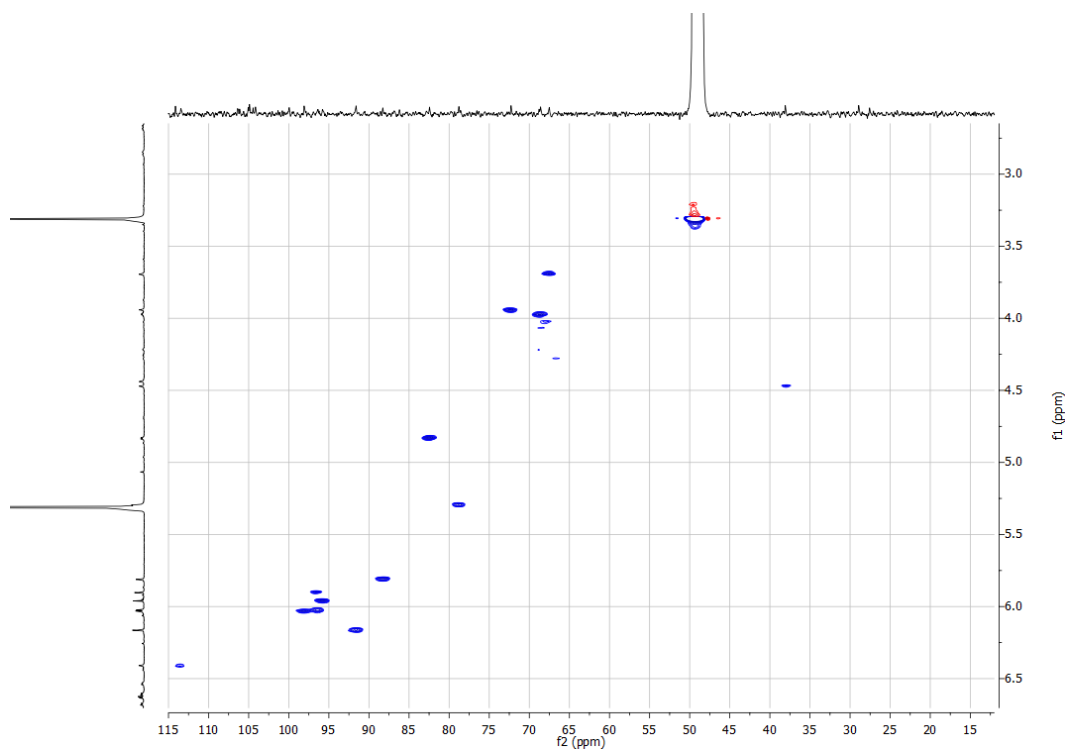


Figure S14. HMBC spectrum of **2** in CD₃OD (255 K).

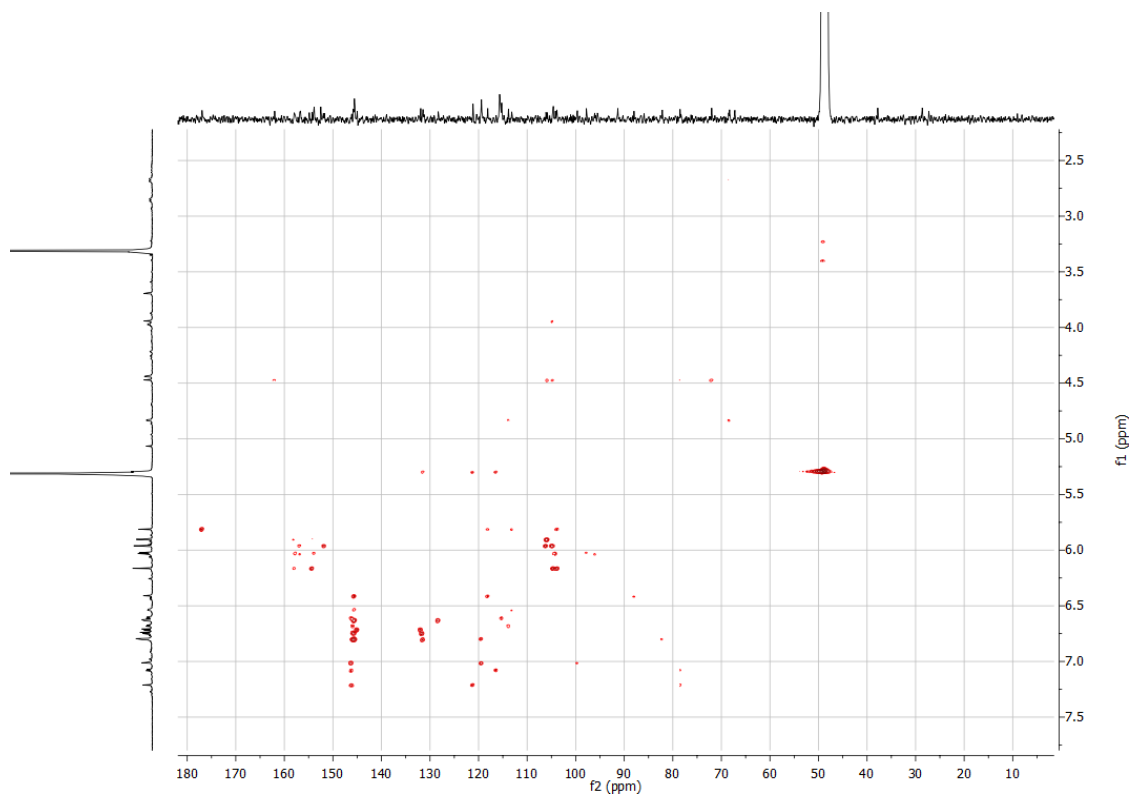


Figure S15. NOESY spectrum of **2** in CD₃OD (255 K).

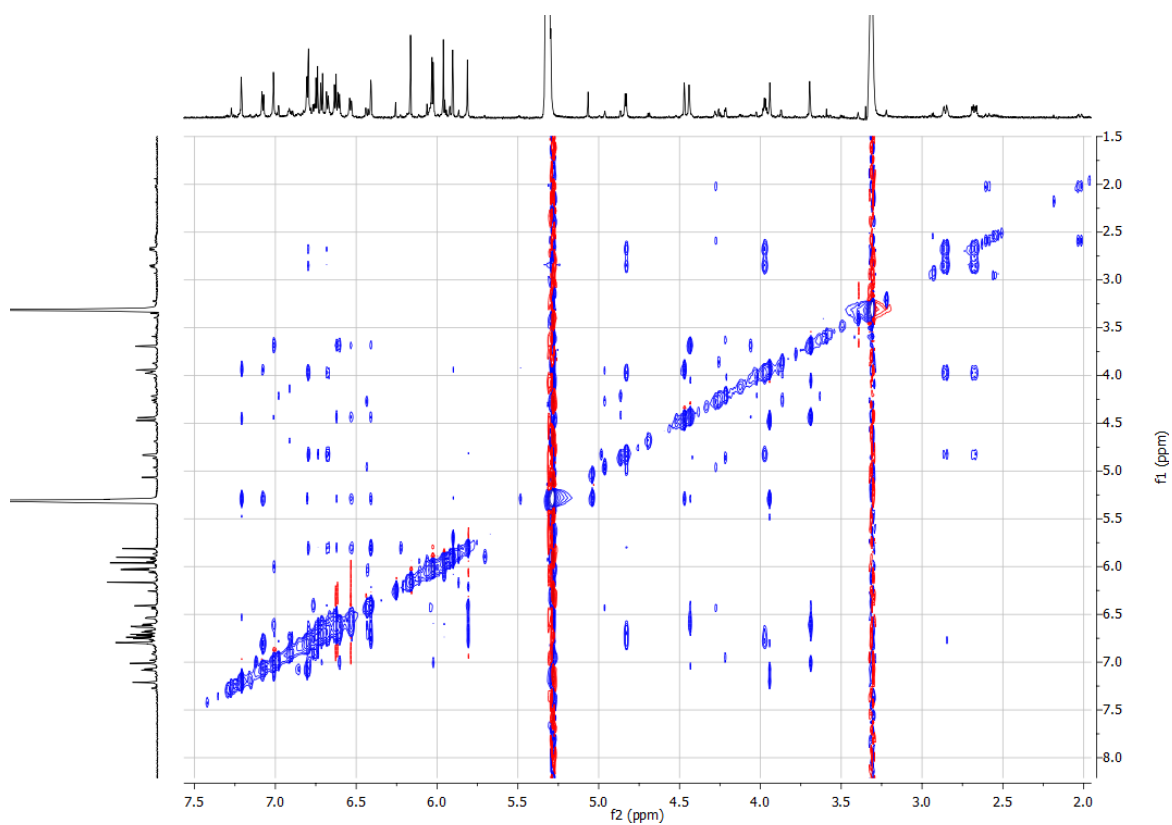


Figure S16. (+)-HRESIMS spectrum of **2**.

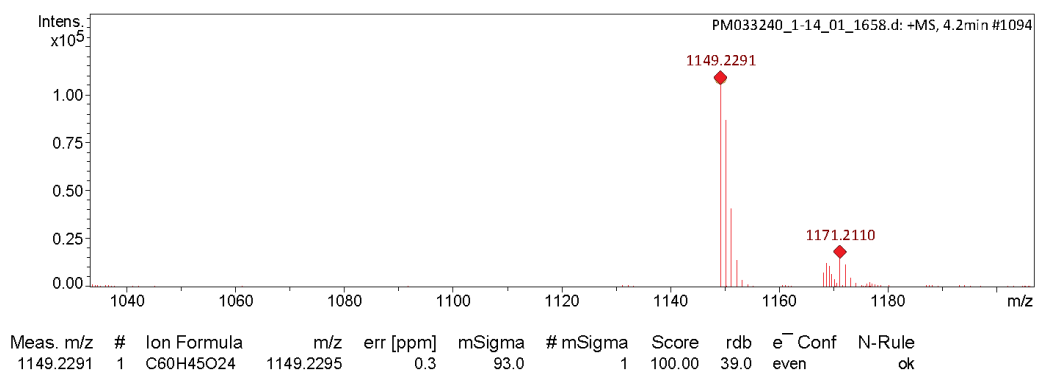


Figure S17. ^1H NMR spectrum of **3** in CD_3OD (800 MHz, 278 K).

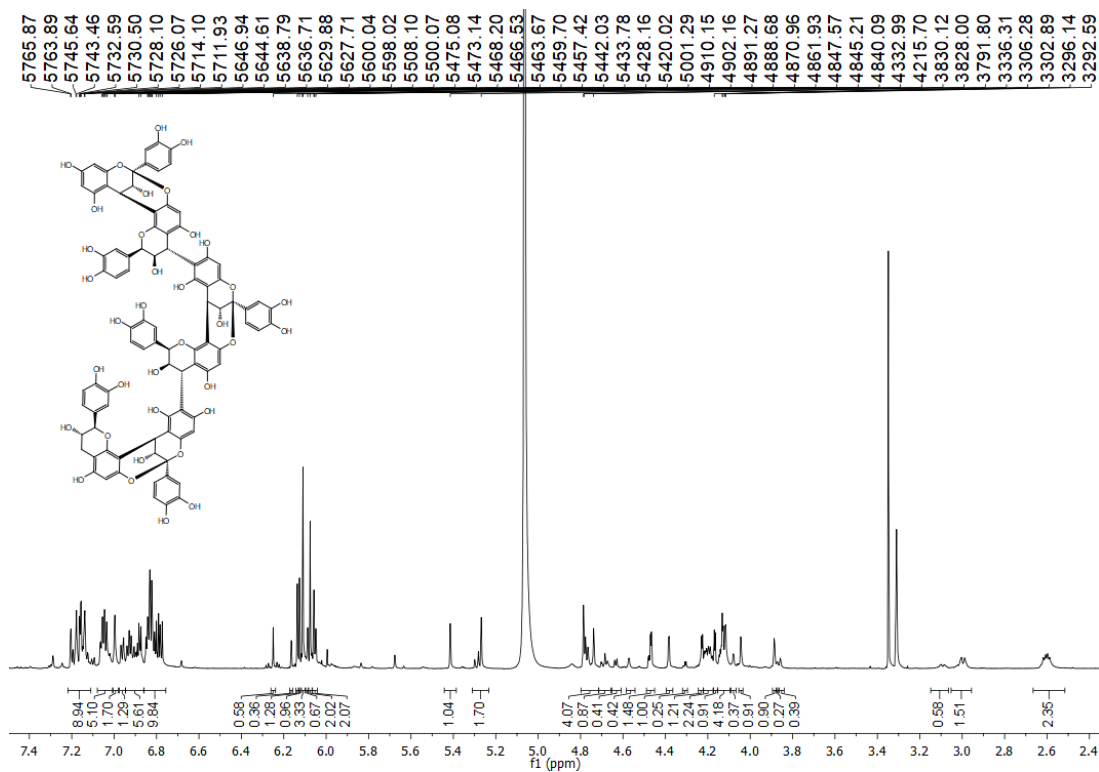


Figure S18. ^{13}C NMR spectrum of **3** in CD_3OD (100 MHz, 278 K).

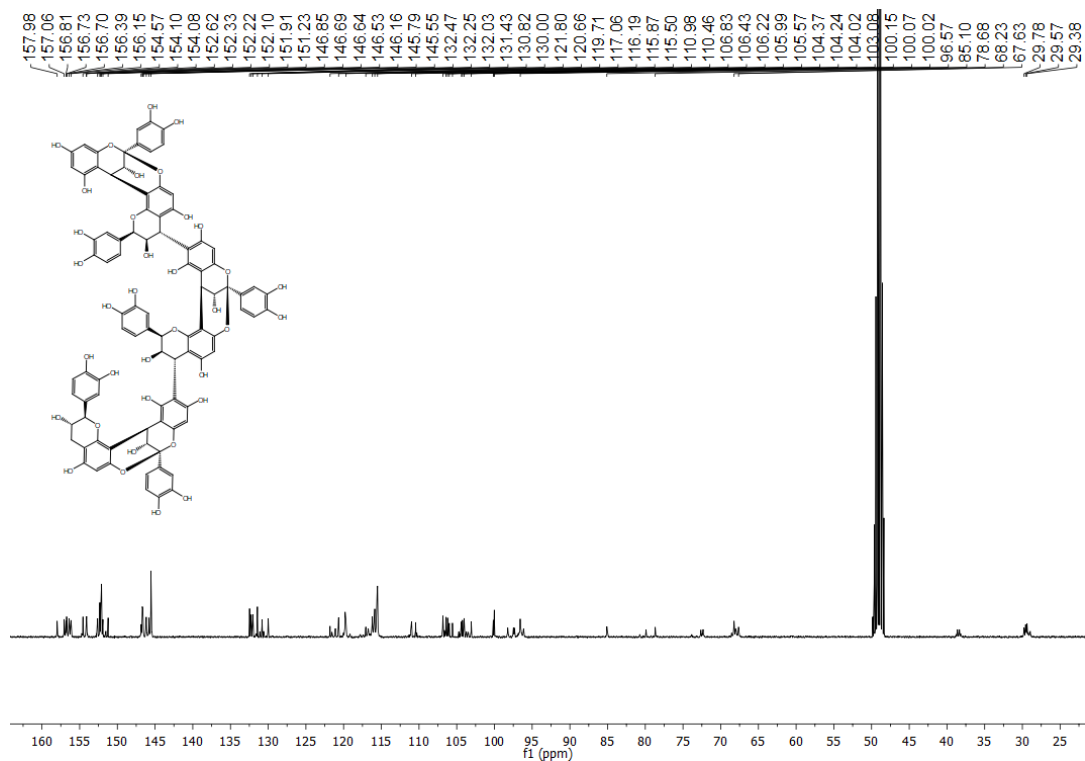


Figure S19. ^1H - ^1H COSY spectrum of **3** in CD_3OD (278 K).

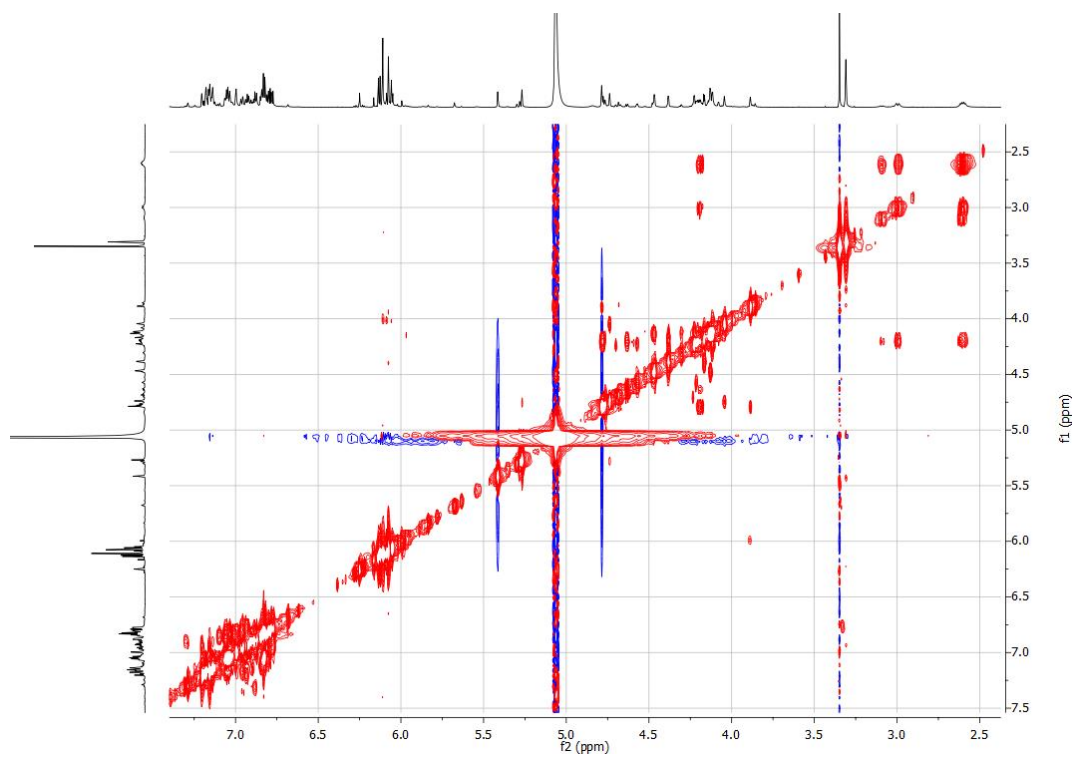


Figure S20. HSQC spectrum of **3** in CD_3OD (278 K).

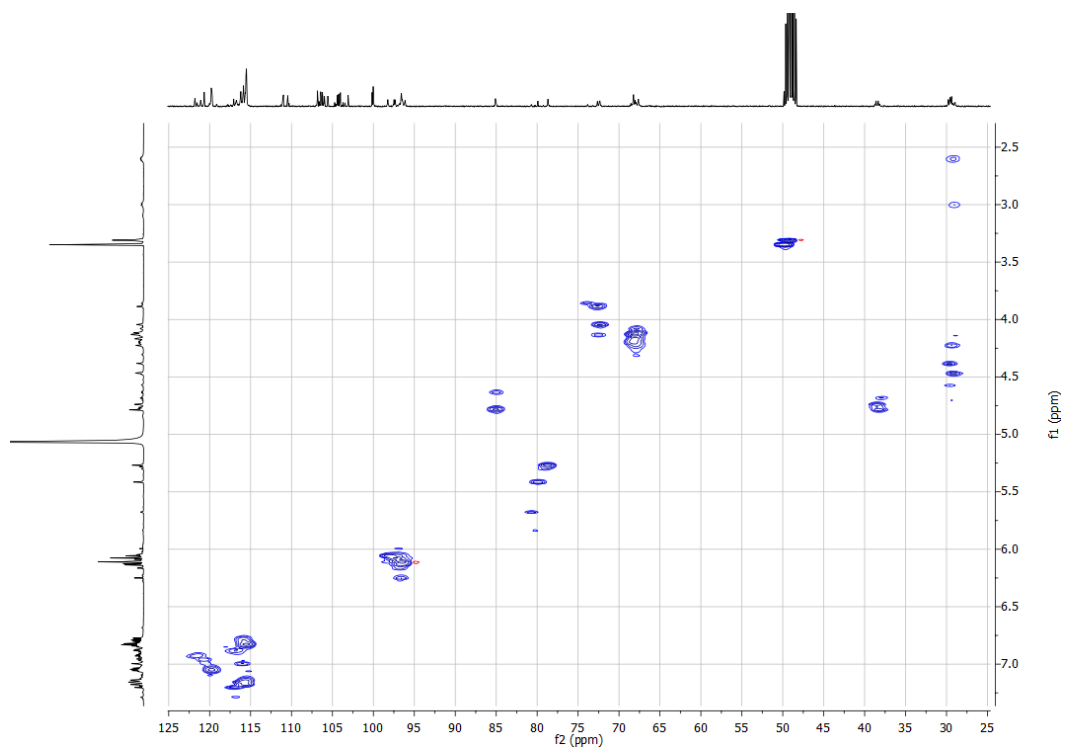


Figure S21. HMBC spectrum of **3** in CD₃OD (278 K).

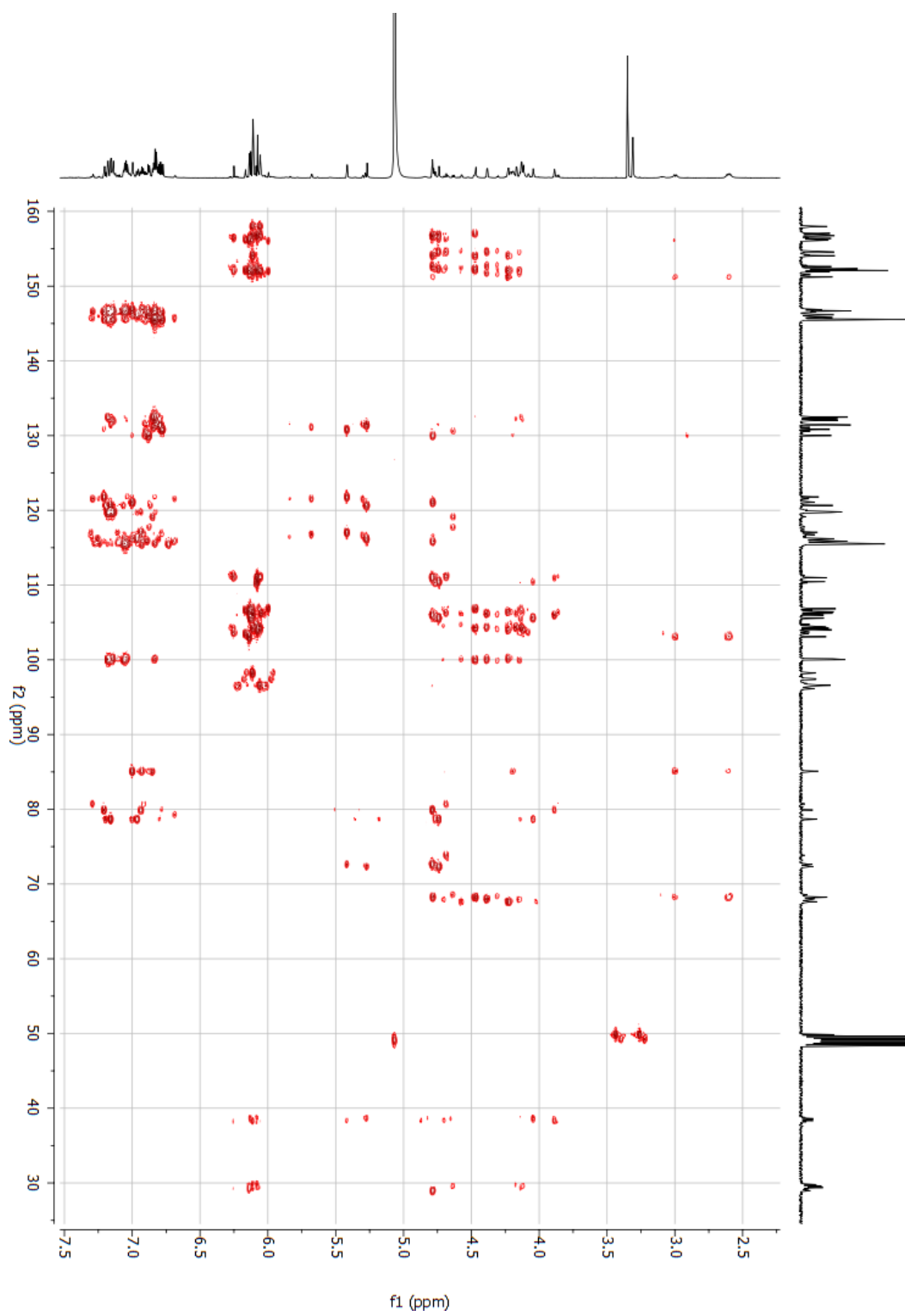


Figure S22. NOESY spectrum of **3** in CD₃OD (278 K).

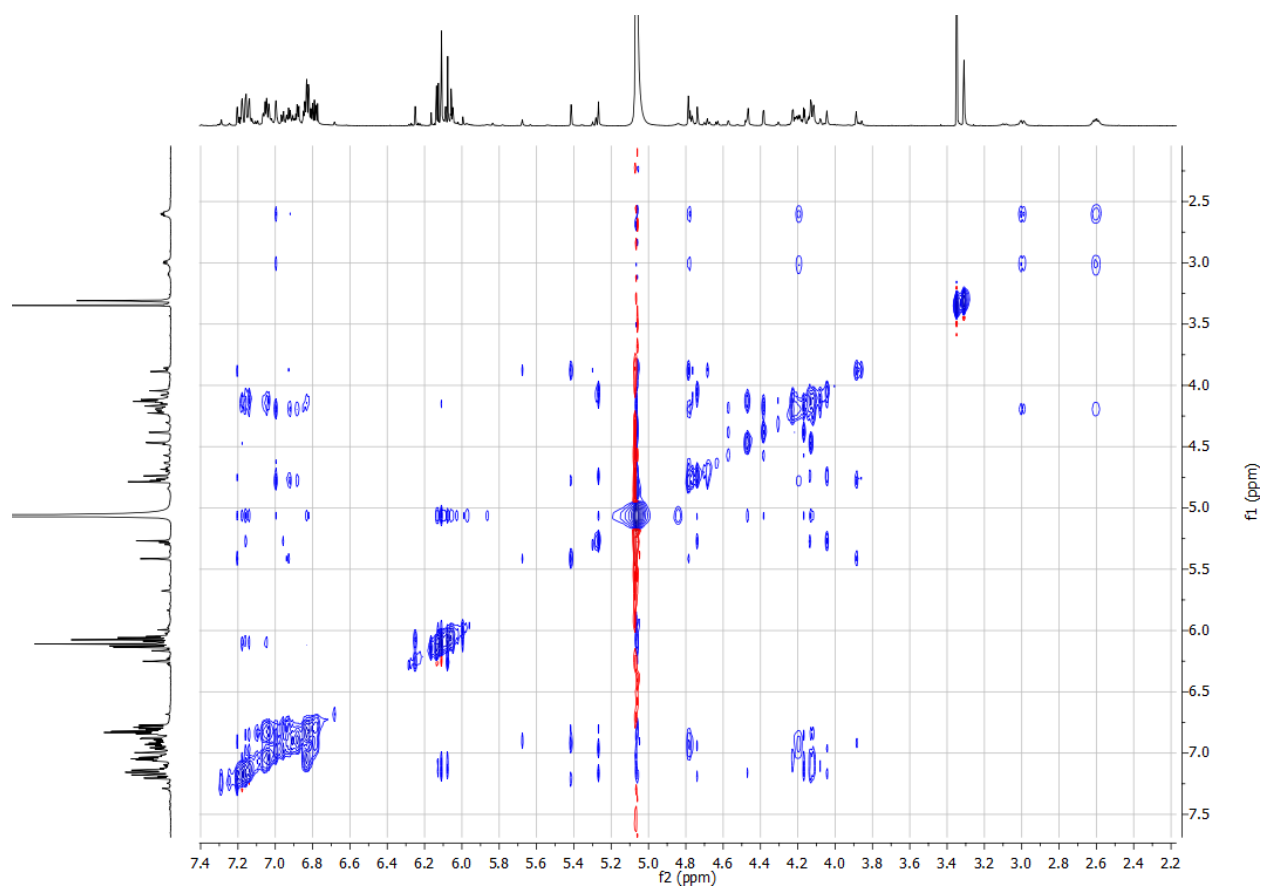


Figure S23. (+)-HRESIMS spectrum of **3**.

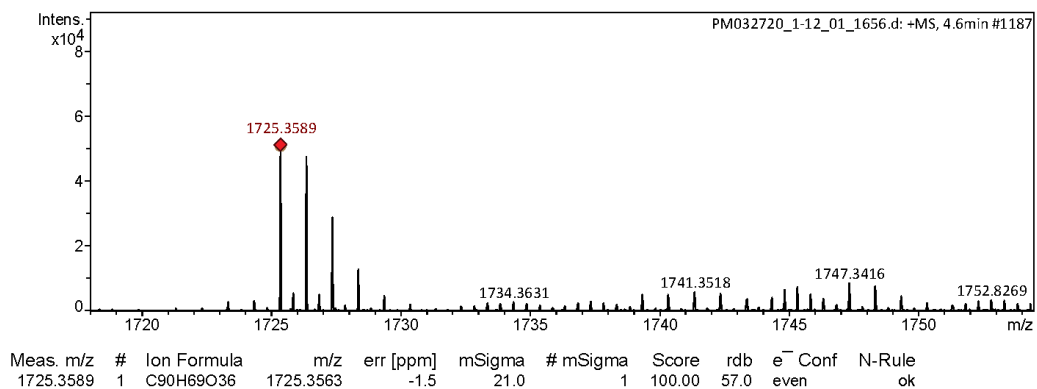


Figure S24. Phloroglucinolysis products of **3** identified by chiral phase HPLC and MS analysis.

